



UNIVERSITY OF LEEDS

This is a repository copy of *Late Cretaceous (Maastrichtian) shallow water hydrocarbon seeps from Snow Hill and Seymour Islands, James Ross Basin, Antarctica*.

White Rose Research Online URL for this paper:
<http://eprints.whiterose.ac.uk/82542/>

Version: Accepted Version

Article:

Little, CTS, Birgel, D, Boyce, AJ et al. (7 more authors) (2015) Late Cretaceous (Maastrichtian) shallow water hydrocarbon seeps from Snow Hill and Seymour Islands, James Ross Basin, Antarctica. *Palaeogeography, Palaeoclimatology, Palaeoecology*, 418. 213 - 228. ISSN 0031-0182

<https://doi.org/10.1016/j.palaeo.2014.11.020>

Reuse

Unless indicated otherwise, fulltext items are protected by copyright with all rights reserved. The copyright exception in section 29 of the Copyright, Designs and Patents Act 1988 allows the making of a single copy solely for the purpose of non-commercial research or private study within the limits of fair dealing. The publisher or other rights-holder may allow further reproduction and re-use of this version - refer to the White Rose Research Online record for this item. Where records identify the publisher as the copyright holder, users can verify any specific terms of use on the publisher's website.

Takedown

If you consider content in White Rose Research Online to be in breach of UK law, please notify us by emailing eprints@whiterose.ac.uk including the URL of the record and the reason for the withdrawal request.



eprints@whiterose.ac.uk
<https://eprints.whiterose.ac.uk/>

1 **Late Cretaceous (Maastrichtian) shallow water hydrocarbon seeps from Snow Hill and**
2 **Seymour Islands, James Ross Basin, Antarctica**

3

4 Crispin T.S. Little^{a*}, Daniel Birgel^b, Adrian J. Boyce^c, J. Alistair Crame^d, Jane E. Francis^d, Steffen
5 Kiel^e, Jörn Peckmann^b, Duncan Pirrie^f, Gavyn K. Rollinson^g and James D. Witts^a

6

7 ^aSchool of Earth and Environment, University of Leeds, Leeds LS2 9JT, UK

8 ^bDepartment of Geodynamics and Sedimentology, Center for Earth Sciences, University of Vienna,
9 1090 Vienna, Austria

10 ^cSUERC, Rankine Avenue, Scottish Enterprise Technology Park, East Kilbride, G75 0QF, UK

11 ^dBritish Antarctic Survey, High Cross, Madingley Road, Cambridge CB3 0ET, UK

12 ^eGeoscience Center, Georg-August University of Göttingen, Geobiology Group, Goldschmidtstrasse
13 3, 37077 Göttingen, Germany

14 ^fHelford Geoscience LLP, Menallack Farm, Trelowarren Mill Barn, Mawgan, Helston, Cornwall, TR2
15 6AE, UK

16 ^gCamborne School of Mines, CEMPS, University of Exeter, Penryn Campus, Cornwall TR10 9FE,
17 UK

18

19 *Corresponding author; telephone/fax number: +44 (0)113 3436621/+44 (0)113 343 5259; email
20 address: earctsl@leeds.ac.uk.

21

22 **Abstract**

23 Fossil hydrocarbon seeps are present in latest Cretaceous (Maastrichtian) volcanoclastic shallow shelf
24 sediments exposed on Snow Hill and Seymour Islands, James Ross Basin, Antarctica. The seeps occur
25 in the Snow Hill Island Formation on Snow Hill Island and are manifest as large-sized, cement-rich
26 carbonate bodies, containing abundant thyasirid bivalves and rarer ammonites and solemyid bivalves.
27 These bodies have typical seep cement phases, with $\delta^{13}\text{C}$ values between -20.4 and -10.7% and

28 contain molecular fossils indicative of terrigenous organic material and the micro-organisms involved
29 in the anaerobic oxidation of methane, including methanotrophic archaea and sulphate-reducing
30 bacteria. On Seymour Island the seeps occur as micrite-cemented burrow systems in the López de
31 Bertodano Formation and are associated with thyasirid, solemyid and lucinid bivalves, and
32 background molluscan taxa. The cemented burrows also have typical seep cement phases, with $\delta^{13}\text{C}$
33 values between -58.0 and -24.6% . There is evidence from other data that hydrocarbon seepage was a
34 common feature in the James Ross Basin throughout the Maastrichtian and into the Eocene. The
35 Snow Hill and Seymour Island examples comprise the third known area of Maastrichtian hydrocarbon
36 seepage. But compared to most other ancient and modern seep communities, the James Ross Basin
37 seep fauna is of very low diversity, being dominated by infaunal bivalves, all of which probably had
38 thiotrophic chemosymbionts, but which were unlikely to have been seep obligates. Absent from the
39 James Ross Basin seep fauna are 'typical' obligate seep taxa from the Cretaceous and the Cenozoic.
40 Reasons for this may have been temporal, palaeolatitudinal, palaeobathymetric, or palaeoecological.

41

42 **Keywords:** Hydrocarbon seeps; palaeoecology; chemosynthetic ecosystems; bivalves; Cretaceous

43

44 **1. Introduction**

45 Hydrocarbon seeps are shallow to deep water (as much as 7 km water depth) sites around the
46 continental margins, in both active and passive settings, where hydrocarbon-rich fluids leak onto the
47 seafloor, forming structures such as pockmarks and mud volcanoes (e.g. Judd and Hovland, 2009, and
48 references therein). Much of the seeping hydrocarbons comprises methane, both of thermogenic and
49 biogenic origin, deriving from underlying thick, organic-rich sedimentary sequences. In the shallow
50 subsurface at seep sites methane is utilized by a consortium of methanotrophic archaea and sulphate-
51 reducing bacteria (SRB) in the anaerobic oxidation of methane (AOM) reaction (e.g. Hinrichs et al.,
52 1999; Boetius et al., 2000; Reitner et al., 2005), leading to the supersaturation of pore fluids with
53 respect to carbonate ions and resulting in the formation of distinctive carbonate deposits with multi-
54 phase carbonate cements and very negative $\delta^{13}\text{C}$ values (e.g. Ritger et al., 1987; Aloisi et al., 2000;

55 Naehr et al., 2007; Haas et al., 2010). Molecular fossils (biomarkers) of the AOM reaction, also with
56 characteristic negative $\delta^{13}\text{C}$ values, are commonly preserved in modern and ancient seep carbonates
57 (e.g. Peckmann et al., 1999; Thiel et al., 1999; Elvert et al., 2000; Bouloubassi et al., 2006; Birgel et
58 al., 2008b). Hydrocarbon seeps support diverse and high-biomass communities of macrofauna, which
59 are dominated by taxa having symbiotic relationships with chemotrophic bacteria (principally
60 methanotrophs and thiotrophs). These taxa include bivalves (e.g. solemyid, vesicomid, lucinid and
61 thyasirid clams, and bathymodiolin mussels) and siboglinid (vestimentiferan) tubeworms (e.g. Paull et
62 al., 1984; Sibuet and Olu, 1998; Levin, 2005; Dubilier et al., 2008). Representatives of the solemyids,
63 lucinids and thyasirids are also common in other environments where reducing sediments
64 predominate (Oliver and Killeen, 2002; Taylor and Glover, 2006; Taylor et al., 2008). There is
65 evidence for a bathymetric control on the ecological and taxonomic structure of modern hydrocarbon
66 seep communities. The number of taxa restricted to seep sites (i.e. obligate taxa) decreases from the
67 slope and deep shelf onto the shallow shelves, such that most obligate chemosymbiotic taxa (such as
68 the vesicomid clams and bathymodiolin mussels) disappear above around 200 m. In contrast, the
69 number of predators and background taxa increases from slope to shallow shelf (Levin et al., 2000;
70 Sahling et al., 2003; Cordes et al., 2007; Dando, 2010). Bathymetric controls are also evident on seep
71 faunas in the Cenozoic and the late Mesozoic (Amano et al., 2010; Kiel, 2010a).

72 The fossil record of seep communities is becoming increasingly well known (e.g. Campbell,
73 2006), especially for the Mesozoic and Cenozoic, and some important macroevolutionary trends are
74 emerging. The Mesozoic fossil seep assemblages contain a variety of dominant obligate ('endemic')
75 taxa, including the dimerelloid brachiopods, the gastropod genus *Paskentana*, and family
76 *Hokkaidoconchidae*, and the bivalve genus *Caspiconcha*, none of which are found in Cenozoic seep
77 communities (Kiel and Little, 2006; Kiel, 2010b, and references therein). Instead, from the Eocene
78 onwards, fossil seep communities contain ubiquitous examples of vesicomids and bathymodiolins,
79 and are structured ecologically much like modern seep communities (Goedert and Squires, 1990; Kiel,
80 2010b). The time period between the latest Mesozoic and the earliest Cenozoic is therefore of interest
81 in elucidating this evolutionary transition, and yet there are very few recorded seep sites of this age:

82 the youngest Tepee Buttes seep deposits of the Western Interior Basin of the USA are Early
83 Maastrichtian (69.1 Ma and older) in age (Metz, 2010), the Sada Limestone seep in Japan is dated as
84 Campanian-Maastrichtian (Nobuhara et al., 2008), and there is one example of a Paleocene seep from
85 California (Schwartz et al., 2003; Kiel, 2013). Further, the macroevolutionary trends in fossil seep
86 faunas so far identified are based largely on data from seeps in the lower latitudes of the Northern
87 Hemisphere; information from the high latitudes in the Southern Hemisphere is particularly sparse,
88 with examples from Late Jurassic of Alexander Island, Antarctica (Kaim and Kelly, 2009) and from
89 the mid- to late Cretaceous of New Zealand (Kiel et al., 2013). This situation is mirrored by the record
90 of modern seeps from Southern high latitudes, which comes from off Chile (e.g. Sellanes et al.,
91 2004), the Hikurangi margin of New Zealand (Baco et al., 2010), and, in Antarctica, the finding in
92 2005 of clusters of dead vesicomimid shells in 850 m water depth in the Weddell Sea after the collapse
93 of the Larsen B Ice Shelf (Domack et al., 2005; Niemann et al., 2009).

94 Here we report an integrated petrological, geochemical (stable isotopes and biomarkers) and
95 palaeontological study of hydrocarbon seeps from latest Cretaceous (Maastrichtian) volcanoclastic
96 shallow shelf sediments exposed on Snow Hill and Seymour Islands, James Ross Basin, Antarctica.
97 The seeps are manifest as large-sized, cement-rich carbonate bodies on Snow Hill Island and micrite-
98 cemented burrow systems on Seymour Island. They are associated with low diversity faunas of
99 thyasirid, solemyid and lucinid bivalves, which we discuss in light of existing ideas about the
100 macroevolutionary history of seep communities.

101

102 **2. Geological setting**

103 2.1. Lithostratigraphy and palaeoenvironments

104 The James Ross Basin is a large extensional sedimentary basin that formed behind the
105 magmatic arc of the Antarctic Peninsula from the late Mesozoic to early Cenozoic (e.g. Pirrie et al.,
106 1997; Crame et al., 2004; Olivero, 2012). The volcanoclastic sediments deposited in this basin are now
107 exposed on the various islands in the James Ross Island area, including Snow Hill and Seymour
108 Islands (subsequently SHI and SI respectively; Fig. 1). On many of the islands the outcrop extent is

109 exceptional (up to 100% on SI), because there is no significant vegetation at this latitude. The Late
110 Cretaceous infill of the James Ross Basin is particularly thick, comprising approximately 2150 m of
111 Campanian and Maastrichtian fine grained sediments, and forms part of the Coniacian to Danian aged
112 Marambio Group (Pirrie et al., 1997; McArthur et al., 2000; Crame et al., 2004; Olivero, 2012). The
113 Maastrichtian part of the group makes up most of the Snow Hill Island Formation (SHIF) and
114 overlying López de Bertodano Formation (LBF) (Fig. 2). The top two units of the SHIF on SHI are
115 the Karlsen Cliffs Member (KCM) below and the Haslum Crag Member (HCM) above (Fig. 2;
116 Zinsmeister, 1998). These two units crop out on the Spath Peninsula at the northern tip of SHI, and
117 along strike on the south western tip of SI (Fig. 1). The KCM consists of mudstones, sandy mudstones
118 and heavily bioturbated fine sandstones with abundant early diagenetic concretions (Pirrie et al.,
119 1997), interpreted by Olivero (2012) to represent sediments formed in a coarsening upwards
120 prograding deltaic wedge. The HCM of Pirrie et al. (1997) is roughly equivalent to the Haslum Crag
121 Sandstone of Olivero (2012) and comprises medium- to coarse-grained cross-stratified and
122 channelized sandstones, passing upwards into intensely bioturbated finer grained sandstones and
123 siltstones, containing fossiliferous concretions (Pirrie et al., 1997). The HCM is separated from the
124 KCM by an unconformity, represented by a thin, framework-supported conglomerate of reworked
125 clasts (Pirrie et al., 1997; Crame et al., 2004). Olivero (2012) interprets the Haslum Crag Sandstone as
126 being forced regressive tidal deposits (Olivero, 2012; fig. 2). The LBF crops out on the eastern side of
127 the Spath Peninsula of SHI (lower part only) and extensively on the western side of SI (full thickness;
128 Fig. 1). The LBF contains the Cretaceous-Paleogene (K–Pg) boundary near its top (Fig. 2; Crame et
129 al., 2004; Olivero, 2012; Tobin et al., 2012). Lithologically the LBF is dominated by intensely
130 bioturbated muddy siltstones, with thin intercalated sandstones and discontinuous concretionary
131 levels, one of which, at locality D5.345.2, was the site of extensive study reported in this paper. The
132 LBF coarsens upwards slightly towards the top of the section where there are some prominent
133 glauconitic sandstones (Crame et al., 2004). According to Olivero (2012) the lower part of the LBF
134 comprises estuarine and shallow marine deposits, the middle part transgressive shelf deposits, and the
135 top part regressive shelf deposits (Olivero, 2012; fig. 2). Palaeotemperature estimates derived from

136 oxygen isotope analysis of molluscan shell material within the LBF indicate mean annual seawater
137 temperatures on the Antarctic shelf ranged from ~5 to - 8°C at this time (Pirrie and Marshall, 1990;
138 Dutton et al., 2007; Tobin et al., 2012), consistent with an overall cooling trend seen globally during
139 the Maastrichtian (e.g. Friedrich et al., 2012).

140

141 2.2. Biostratigraphy and chronostratigraphy

142 Precise dating of the James Ross Basin sediments to lower latitude sections is hampered by a
143 number of issues which make correlation to well-dated Late Cretaceous IODP/DSDP ocean drill-
144 cores and stratigraphic sections in the northern hemisphere problematic. Both macro and microfossil
145 faunas and floras show a high degree of endemism (e.g. Macellari, 1986; Zinsmeister and Macellari,
146 1988; Pirrie et al., 1997; Olivero and Medina, 2000; Crame et al., 2004; Bowman et al., 2012;
147 Olivero, 2012), and several key groups useful for biostratigraphy elsewhere such as certain ammonites
148 and inoceramid bivalves, either disappear from the Antarctic record during the Campanian
149 (Zinsmeister and Feldmann, 1996; Crame et al., 1996; Crame and Luther, 1997; McArthur et al.,
150 2000; Olivero and Medina, 2000; Olivero, 2012) or are absent from the James Ross Basin record
151 entirely. Dinoflagellate cysts may provide the best opportunity for microfossil biostratigraphy of the
152 basin due to the paucity of other groups such as foraminifera (Pirrie et al, 1997; Bowman et al., 2012;
153 2013), but correlation to lower latitudes is still problematic and key stratigraphic sections such as
154 those on SHI await revision.

155 In terms of macrofossils, ammonites appear to hold the most promise for biostratigraphic
156 zonation and comparison with other sections. They are among the most common fossils found
157 throughout the Late Cretaceous sequence (Macellari, 1986; Olivero, 1984; 1988; 1992; 2012; Crame
158 et al., 2004; Kennedy et al., 2007) and provide an important stratigraphic reference for correlating
159 sections across the entire basin (Pirrie et al, 1997; Olivero and Medina, 2000; Crame et al., 2004;
160 Olivero et al., 2008; Olivero, 2012). Olivero and Medina (2000) and Olivero (2012) divide the James
161 Ross Basin into 14 distinct ammonite assemblages, based mainly on the stratigraphic distribution of
162 the family Kossmaticeratidae, which contains many endemic taxa. The KCM and HCM occur in

163 assemblage 10, which is also present in the Cape Lamb Member of the SHIF on Vega Island. Detailed
164 stratigraphic range data for ammonite taxa from the KCM and HCM have never been illustrated, but
165 the fauna appears to be dominated by specimens belonging to the kossmaticeratid genera *Gunnarites*,
166 most probably the highly variable *Gunnarites antarcticus*. Other ammonites reported from the KCM
167 and HCM are indicative of a Late Campanian to Maastrichtian age when compared with lower
168 latitude sections, such as those in South America, South Africa, Australia and New Zealand (Charrier
169 and Lahsen, 1968; Henderson, 1970; Kennedy and Klinger, 1985; Henderson and McNamara, 1985;
170 Walaszczyk et al., 2009; Salazar et al., 2010; Stinnesbeck et al., 2012). They also form a distinctly
171 different assemblage to those found stratigraphically higher in the LBF on SI (see below and Crame et
172 al., (2004)). This biostratigraphic interpretation is consistent with strontium isotope data from the age-
173 equivalent Cape Lamb Member on Vega Island (Crame et al., 1999; McArthur et al., 2000), which
174 suggests an early Maastrichtian age for this unit.

175 Biostratigraphic zonation of the LBF on SI using ammonites is similarly hampered by the
176 dominance of endemic kossmaticeratid taxa. The studied concretion-rich layer at locality D5.345.2 is
177 located in ammonite assemblage 11 of Olivero and Medina (2000) and Olivero (2012). A single well-
178 preserved specimen of *Maorites seymourianus* was found at this locality (Fig. 5D), whilst nearby
179 equivalent horizons have also yielded specimens of *Maorites* (probably *seymourianus*) and *Kitchinites*
180 *darwini* (see also Macellari, 1986). Other reported taxa from this stratigraphic interval include
181 *Diplomoceras cylindraceum*, *Pseudophyllites loryi* and *Neophylloceras* sp. (Olivero, 2012). All of
182 these taxa are consistent with a Maastrichtian age for these deposits. Strontium isotope data
183 (McArthur et al., 1998; Crame et al., 2004), and recent biostratigraphic studies using marine
184 palynology (Bowman et al., 2012; 2013), suggest all of the HCM and LBF exposed on SI below the
185 K–Pg boundary are early to latest Maastrichtian in age when compared to other Southern Hemisphere
186 sections. A recent magnetostratigraphic study of the LBF (Tobin et al., 2012) identified several
187 magnetic polarity reversals which can be correlated with both lower latitude sections and a recently
188 revised global Maastrichtian timescale (e.g. Husson et al., 2011; Gardin et al., 2012; Voigt et al.,
189 2012), as well as new age models for the SI succession (Bowman et al., 2013). This work suggests the

190 Cretaceous portion of the LBF on SI spans magnetochrons C31R through to C29R and was therefore
191 deposited between ~70 and 66 Ma – the currently accepted date of the K–Pg boundary (Husson et al.,
192 2011; Voigt et al., 2012; Tobin et al., 2012). Based on application of the data presented in Tobin et al.
193 (2012) to measured sections used herein (see also Bowman et al. 2013) the concretion-rich layer at
194 locality D5.345.2 occurs somewhere in the upper part of chron C31R, indicating a date of ~69 Ma
195 (Husson et al., 2011; Voigt et al., 2012; Fig. 2).

196

197 **3. Materials and methods**

198 Rock samples and fossils were collected from SHI and SI during a series of field seasons to
199 the James Ross Basin area by the British Antarctic Survey (BAS) and collaborators from ~1994 to
200 2007 and are stored in the BAS collections and those in the School of Earth and Environment,
201 University of Leeds. A subset of these samples from the carbonate-cemented layers and associated
202 fossils on SHI and the concretion-rich layer at locality D5.345.2 on SI were selected for additional
203 analysis (Table 1). Additional samples from SI come from the Zinsmeister collection housed in the
204 Paleontological Research Institution, Ithaca, New York, USA (Table 1).

205

206 **3.1. Petrography**

207 Three samples from SHI were analysed petrographically at Helford Geoscience LLP (Table
208 1). Multiple uncovered polished thin sections were prepared from the samples. Each thin section was
209 scanned and examined under polarised light microscopy, using cathodoluminescence (CL) and
210 following carbonate staining. The mineralogy and texture of three representative thin sections was
211 quantified using automated SEM-EDS analysis using QEMSCAN[®] technology (see Pirrie et al., 2004,
212 2014). The sections were carbon coated and then the whole area of each thin section was scanned
213 using a 10 µm beam stepping interval; subsequently smaller areas of the thin section were also
214 measured using a 5 µm beam stepping interval. Five samples from SI were analysed petrographically
215 using covered and uncovered thin sections under light microscopy at the University of Leeds and
216 Georg-August Universität Göttingen (Table 1), and one of these was micro-drilled for X-ray

217 diffraction (XRD) analysis at the University of Leeds using a Bruker D8 with a Cu K alpha source
218 and configured to a vertical theta/2 theta Bragg-Brentano reflection stage, and with a Lynxeye
219 detector. Phase identification was achieved using Bruker's EVA software with the ICDD PDF2
220 database.

221

222 3.2. Carbonate stable carbon and oxygen isotopes

223 Samples from the petrographic specimens and others from SHI and SI were micro-drilled to
224 produce powders, and were analysed at the Scottish Universities Environmental Research Centre, East
225 Kilbride and the Georg-August Universität Göttingen. At East Kilbride CO₂ was quantitatively
226 released from the powdered samples by standard in vacuo digestion with 100% phosphoric acid at
227 25°C. Gases thus produced were analysed on a VG SIRA 10 mass spectrometer, monitoring mass to
228 charge ratios of 44, 45 and 46. Analytical raw data were corrected using standard procedures (Craig,
229 1957). The error of reproducibility, based on complete analysis of internal standards (including acid
230 digestion) was ±0.1‰ for δ¹³C values, and ±0.2‰ for δ¹⁸O values. At Göttingen, the powdered
231 samples were reacted with 100% phosphoric acid at 75°C using a Finnigan Kiel IV Carbonate Device
232 attached to a Finnigan DELTA V PLUS mass spectrometer. Reproducibility was checked by replicate
233 analysis of laboratory standards and was better than ±0.05‰. All isotope data are given as δ values in
234 per mil (‰) relative to the Vienna Pee Dee belemnite (V-PDB) standard.

235

236 3.3. Lipid biomarkers

237 A single sample (Sn1-1) from SHI, previously drilled for isotope analysis, was analysed for
238 biomarkers at the Centre of Marine Environmental Sciences (MARUM), Bremen University (Table
239 1). The preparation and decalcification procedure was performed after a method described in Birgel et
240 al. (2006b). After the saponification procedure with KOH (6%) in methanol, the sample was extracted
241 with a microwave extraction system (CEM MARS X) at 80°C and 300 W with a 3:1
242 dichloromethane-methanol mixture. The separation of the total lipid extract was performed after
243 Birgel et al. (2008a). The resulting hydrocarbons and carboxylic acids fractions were measured with a

244 Thermo Electron Trace MS gas chromatograph-mass spectrometer, equipped with a 30 m Rxi-5 MS
245 fused silica column (0.25 mm inside diameter, 0.25 μm film thickness), using helium as the carrier
246 gas. The temperature program was: 60°C, 1 min isothermal; from 60 to 150°C at 10°C/min, from 150
247 to 320°C at 4°C/min; 22 min isothermal at 320°C. Identification of individual compounds was based
248 on retention times and published mass spectra. Compound-specific carbon isotope analysis of the
249 molecular fossils was performed with a Thermo Electron Trace GC Ultra connected via a Finnigan
250 combustion interface-II to a Finnigan MAT 252 mass spectrometer. Conditions of the gas
251 chromatograph were identical to those described above. Carbon isotopes are given as δ values in per
252 mil (‰) relative to the Vienna Peedee belemnite (V-PDB) standard. Each measurement was
253 calibrated using several pulses of CO₂ with known isotopic composition at the beginning and end of
254 the run. Instrument precision was checked with a mixture of n-alkanes (C₁₅ to C₂₉) of known isotopic
255 composition. The analytical standard deviation was < 0.8‰.

256

257 **4. Results**

258 4.1. Carbonate bodies and 'Thyasira' occurrences on Snow Hill Island

259 Specimens of the large thyasirid bivalve '*Thyasira*' townsendi are common in the lower part
260 of the type section of the KCM on the Spath Peninsula at Thyasira Hill (64.3748°S, 56.9807°W; Fig.
261 1). Here the first '*T.*' townsendi are found at the 30 m mark in BAS section DJ.616 of Pirrie et al.
262 (1997) occurring initially as articulated singletons, both in situ (i.e. with the plane of the dorsal
263 commissure vertical) and displaced to lie on one valve or the other. Numbers of specimens increases
264 very rapidly up section to reach, in places, an estimated density of >120/m² (Fig. 3C). Between
265 approximately 30 and 65 m in section DJ.616 clusters of '*T.*' townsendi are increasingly associated
266 with patches of pale blue-grey carbonate cementation which serve to accentuate the regular, planar
267 bedding (Fig. 3B,D). Initially the cemented regions are 20 to 30 cm thick and 50 to 100 cm in width
268 but at higher levels the beds are more continuous and weather out to form the peak of a prominent
269 structure 60 m in height that forms the summit of Thyasira Hill (Figs. 3A, 4A,C). This feature is
270 located approximately 500 m SW of Nordenskjöld's Hut. At Thyasira Hill the carbonate cemented

271 beds are 30 to 75 cm thick and sheet-like on the scale of exposure. The internal texture of the best
272 cemented beds is very much that of a shell bed that in places verges into a coquina (Figs. 3E, 4C).
273 Many of the 'T.' *townsendi* shells (Fig. 5G) are in growth position, but it is noticeable that they rarely
274 touch each other (Fig. 4C, 5A); others are clearly ex-situ and some of these are broken. A number of
275 small ammonites, and ammonite fragments, are also preserved in the cemented layers (Fig. 3E). These
276 are mostly referable to *Gunnarites* (Fig. 5E) and occasional *Anagaudryceras* and many appear to be
277 juveniles. Their disposition is such as to suggest that they could have been current-swept into the
278 'Thyasira' layers. The interbeds between the well-cemented layers have yielded isolated articulated
279 specimens of 'T.' *townsendi* together with small ammonites, including *Jacobites anderssoni* (Fig. 5F),
280 and possible *Gunnarites bhavaniformis* (Fig. 5E), and scattered tube specimens of the serpulid worm
281 *Austrorotularia* sp. About 200 m across a small valley to the South of Thyasira Hill at the same
282 stratigraphic level are approximately 12 topographic knolls up to 10 m tall and ~5 m wide (Fig.
283 3B,D), which represent carbonate cemented patches that have been exhumed by weathering from the
284 enclosing fine-grained sediments of the KCM. These knolls have similar lithologies and faunal
285 content to Thyasira Hill, including the ammonite *Gunnarites antarcticus*, the solemyid bivalve
286 *Solemya rossiana* and an indeterminate high-spined gastropod. Carbonate cemented 'Thyasira' layers
287 and patches continue between 65 and 80 m in the section DJ.616, but are not observed in the topmost
288 20 to 25 m. It should be emphasized that the well-cemented 'Thyasira' patches and layers are
289 markedly discontinuous both laterally and vertically. They occur through an approximately 50 m thick
290 section of DJ.616 (i.e. ~30 and 80 m), but at no other stratigraphic level within the KCM. Equally,
291 they cannot be traced laterally in the extensive headwall of the small valley system immediately to the
292 SW of Nordenskjöld's Hut. The cementation is patchy and discontinuous over perhaps a 100 m
293 distance horizontally and a 50 m stratigraphical thickness.

294

295 4.2. Carbonate concretions and 'Thyasira' occurrences on Seymour Island

296 'Thyasira' *townsendi* occurs intermittently in laterally discontinuous layers, usually within a
297 distinctive dark sulphurous mudstone facies, throughout the rest of the nearly 1500 m thick

298 Maastrichtian succession on SHI and SI. In these layers '*T.*' *townsendi* often occurs together with
299 articulated specimens of the lucinid bivalve '*Lucina*' *scotti* (Fig. 5J) and/or the solemyid bivalve
300 *Solemya rossiana*. However, unlike in the KCM, the stratigraphically later '*T.*' *townsendi* layers in the
301 HCM and LBF are not associated with well-cemented large carbonate deposits. The '*T.*' *townsendi*
302 layers occur in several places in the LBF on SI (Table 1). One of these, at locality D5.345.2, 458 m
303 above the basal unconformity with the HCM (Fig. 2), contains scattered carbonate-cemented
304 concretions together with abundant specimens '*T.*' *townsendi* (Fig. 5H) and *S. rossiana* (Fig. 5K) and
305 some examples of the ammonite *Moarites seymourianus* (Fig. 5D). There are also large numbers of
306 the nuculid bivalve *Leionucula suboblonga*, small examples of the trigoniid *Oistrigonia pygoscelium*
307 and the gastropod "*Cassidaria*" *mirabilis*. Horizons immediately adjacent to D5.345.2 also yield
308 examples of the bivalves *Nordenskjoldia nordenskjoldi*, *Cucullaea antarctica*, and a small
309 indeterminate veneroid. These molluscan taxa are a good representation of the 'background' benthic
310 molluscan fauna found throughout this portion of the LBF on SI (e.g. Crame et al., 2004). The last
311 occurrence of the distinctive '*T.*' *townsendi* facies occurs in section line DJ.953, 48 m below the K–Pg
312 boundary in the LBF (Figs. 1 and 2). However, a single specimen of '*T.*' *townsendi* was recently
313 collected from the 237-250 m level in the Paleocene Sobral Formation, i.e. ~300 m above the K–Pg
314 boundary.

315 The concretions at locality D5.345.2 are fairly diverse in size and shape. Some have a roughly
316 cylindrical shape, are between 11 and 18 mm in diameter and up to 39 mm in length (Fig. 5B). These
317 are largely composed of dark grey fine-grained sediments cemented by micrite with a later,
318 weathering rind of gypsum, but some also have internal infillings of fibrous calcite cements (Fig. 6B).
319 Other concretions are roughly circular, between 31 and 49 mm in diameter and have pale-coloured
320 *Planolites*-like burrows on their surfaces (Fig. 5B). Internally these concretions are formed of dark
321 grey fine-grained sediments, within which similar burrows can often be seen.

322

323 4.3. Petrography

324 The samples (DJ.731.14 and DJ.633.3) from carbonate cemented bodies in the KCM on SHI
325 comprise muddy to silty very fine grained sandstones composed of angular grains of detrital quartz,
326 plagioclase and microcline, along with abundant biotite and diagenetic glauconite, minor muscovite,
327 and occasional framboidal pyrite and wood fragments, including examples of Cupressinoxylon or
328 Podocarpoxyton (Figs. 6A,C,D; 7C). Texturally the sediments have a bioturbated fabric; locally with
329 a peloidal texture with oval faecal pellets. The sediments are tightly cemented by a non-ferroan
330 micritic to microsparry calcite (Figs. 6A,C,D; 7C), and this commonly causes splaying of biotite
331 micas with the growth of calcite cements parallel to the mineral cleavage. This cement phase we label
332 m1 is thought to correspond to similar phases in Kiel et al. (2013). The micrite and microspar are
333 intergrown with and post-dated by two main generations of ferroan calcite cement, which are bright
334 orange luminescent under CL (Fig. 7C). Cross-cutting the sediments are pipe-like structures (which
335 we interpret as fluid conduits in section 5) up to several centimetres in length, filled by numerous
336 generations of carbonate cements (Figs. 6A,C,D; 7A-C). These cements are nucleated onto the
337 surrounding sandstones and also overgrow faecal pellets. The cement infills within these pipe-like
338 structures are complex, with up to six zones per pipe of a non-ferroan, fibrous calcite cement with
339 banded and botryoidal textures (termed bbc; Fig. 7A,B). Under CL this fibrous cement shows
340 complex zones of alternating bright and less bright orange luminescence (Fig. 7C). QEMSCAN[®]
341 mapping shows that within some of the pipe fills there is a zone of carbonate cement containing Fe
342 and Mn (probably ankerite) which post-dates, and is in turn post-dated by, fibrous calcite cements
343 (Figs. 6C-D; 7B). In addition, a zone of Mg-rich carbonate (possibly dolomite) occurs towards the
344 centre of the pipes, post-dating the calcite cements and in turn being post-dated by equant, drusy
345 mosaic ferroan calcite cements (ec) and/or microcrystalline calcite cement (m2). The QEMSCAN[®]
346 analysis shows that nearly 80% of the area of the measured thin section is composed of carbonate
347 cements (Fig. 6C-D). Diagenetic pyrite forms approximately 0.5% of the area of the measured thin
348 section.

349 The sediment infills and carbonate cements in the two articulated '*Thyasira townsendi*
350 specimens from Thyasira Hill, SHI (samples DJ.616.22 and DJ.616.34), and the articulated '*T.*'

351 townsendi specimen (PRI 61054) from SI (Table 1) are petrographically very similar to the samples
352 described above, with sparry to microsparry/micritic calcite cemented silty and peloidal sediment,
353 overgrown with multiple zones of fibrous calcite cements, which grow into the open space in the
354 centre of the articulated valves. These cements in the SI 'T.' townsendi specimen appear black in
355 colour to the naked eye. The shells of 'T.' townsendi specimens from SHI are recrystallized to sparry
356 calcite and there is no trace of original microstructures.

357 The concretions at locality D5.345.2 on SI have similar petrographic characteristics to the
358 SHI KCM samples. Where present, multiple generations of banded and botryoidal fibrous calcite
359 cements (bbc) fill centimetre-scale pipe-like structures within the concretions (Figs. 6B; 7D). The
360 bands of fibrous cement are either of a yellowish colour (ybbc) or are translucent (tbbc); although
361 these phases formed recurrently in places, resulting in an intimate intercalation, the former phase
362 tends to predate the latter. In places adjacent to the walls of the pipes the fibrous cements have been
363 recrystallized (rbbc) to equant calcite (Fig. 7D).

364

365 4.5. Carbonate stable carbon and oxygen isotopes

366 The $\delta^{13}\text{C}$ and $\delta^{18}\text{O}$ values for the SHI and SI carbonates fall into two distinct clusters (Table
367 2, Fig. 8). The SI concretion matrices and fibrous calcite cements, and the fibrous calcite cements
368 from inside articulated bivalves have negative $\delta^{13}\text{C}$ values between -58.0 and -24.6‰ , and $\delta^{18}\text{O}$
369 values between -2.3 and 2.1‰ . The SHI carbonate $\delta^{13}\text{C}$ values are less negative, with most clustering
370 between -20.4 and -10.7‰ . These include all the fibrous calcite cements, the Thyasira Hill cemented
371 sediment, the micro-sparry calcite cement sample and three of the five sparry calcite cement samples.
372 The other two sparry calcite cements have $\delta^{13}\text{C}$ values that straddle the single analysed 'Thyasira'
373 townsendi shell value of -4.1‰ . The $\delta^{18}\text{O}$ values of the SHI carbonates are mostly more negative
374 than the SI carbonates, being between -8.3 and -1.6‰ .

375

376 4.6. Molecular fossils and their compound-specific isotopes

377 The hydrocarbon fraction (Fig. 9A) of the studied sample (Sn1-1) from Thyasira Hill, SHI is
378 predominantly composed of n-alkanes ranging from n-C₁₆ to n-C₃₁ without a preferential distribution
379 of odd or even chains. The n-alkanes maximize at intermediate chain lengths (n-C₂₂ to n-C₂₄) and long
380 chain n-alkanes (>n-C₂₇) are present only in minor amounts. In addition to the n-alkanes, multiple
381 branched alkanes, the so-called isoprenoids, are abundant, although in lesser amounts than the n-
382 alkanes. Among the identified isoprenoids are the two head-to-tail linked isoprenoids 2,6,10,14-
383 tetramethylpentadecane (pristane) and 2,6,10,14-tetramethylhexadecane (phytane). The latter
384 compound is co-eluting with the tail-to-tail linked isoprenoid 2,6,11,15-tetramethylhexadecane
385 (crocetane). Crocetane makes up approximately 40% of the mixed crocetane/phytane peak. We
386 identify a second tail-to-tail linked isoprenoid as 2,6,10,15,19-pentamethylcosane (PMI). In addition,
387 trace amounts of the head-to-head linked isoprenoid 3,7,11,15,18,22,26,30-octamethyldotriacontane
388 (acyclic biphytane) are present.

389 The carboxylic acid fraction of the sample (Fig. 9B) is composed predominantly of n-fatty
390 acids (FA) with 12 to 32 carbon atoms. The FA show an odd over even predominance. Short-chain
391 FA maximize at n-C₁₆ FA. Intermediate and long-chain FA (n-C₂₀ to n-C₂₈) show only slightly
392 varying contents, whereas the chains with 29 or more carbons are only present in trace amounts. Other
393 than the straight-chain FA, short-chain terminally-branched FA were identified, including iso-C₁₄ FA,
394 iso- and anteiso-C₁₅ FA, and iso-C₁₆ FA. In addition, α,ω -diacids from C₁₆ to C₂₆ were identified (Fig.
395 9B). Isoprenoidal biphytanic diacids with 0 to 2 cyclopentane rings were found in trace amounts, with
396 acyclic and bicyclic biphytanic diacids (40% each of all biphytanic diacids) predominating over the
397 monocyclic biphytanic diacid (20% of all biphytanic diacids). Other than aliphatic compounds, a
398 series of hopanoic acids were found, ranging from C₃₁ to C₃₄ and maximizing at C₃₂. All hopanoic
399 acids were present as their 17 β (H),21 β (H)-isomers. The $\delta^{13}\text{C}$ values of all the measured n-alkanes (n-
400 C₁₈ to n-C₂₆) revealed values of -27‰ and -26‰ ; the contents of long-chain n-alkanes were too low
401 to measure stable carbon isotopes. The mixed crocetane/phytane peak has a value of -61‰ , whereas
402 PMI shows a value of -83‰ . Biphytane was not measured for its isotopic composition because of its
403 low concentration in the sample. The $\delta^{13}\text{C}$ values of n-fatty acids range from -40‰ (n-C₁₆ FA) to

404 -29‰ (n-C₂₈ FA). The α,ω -diacids have values of -29‰ (C₂₄-diacid) to -25‰ (C₁₈-diacid). The
405 terminally-branched FA showed the strongest variation in $\delta^{13}\text{C}$ values ranging from -57‰ (anteiso-
406 C₁₅ FA) to -35‰ (iso-C₁₄ FA). The $\delta^{13}\text{C}$ values of the hopanoic acids and biphytanic diacids were not
407 measured because they occurred in very low concentrations.

408

409 **5. Interpretations**

410 5.1. Snow Hill Island carbonate deposits as hydrocarbon seeps

411 We interpret the deposits of carbonate cemented sediments occurring in the KCM on SHI as
412 having being formed by hydrocarbon seepage, because of their morphology, petrography, organic
413 biomarkers and stable isotope values. The wide variation in size of the deposits, and, in particular,
414 their lack of lateral persistence, is a common feature of modern and fossil hydrocarbon seep deposits
415 (e.g. Han et al., 2004; Agirrezabala et al., 2013). We suggest the increasing thickness of the deposits
416 in the KCM on Spath Peninsula up to the level of Thyasira Hill shows increasing flux of hydrocarbons
417 during the deposition of the KCM, as there is no obvious change in sedimentation rate at the time.
418 This increasing flux presumably explains the local increases in numbers of *Thyasira townsendi*
419 specimens in the deposits up-section. The *Thyasira townsendi* layers below the first occurrence of
420 carbonate cemented layers may indicate incipient seepage within the basin (see section 6.1).

421 The $\delta^{13}\text{C}$ value from the single analysed *T. townsendi* shell from the KCM indicates a
422 carbon source from seawater bicarbonate, and not from hydrocarbons, an interpretation which is
423 consistent with the observation that bivalves largely (but not exclusively; Lartaud et al., 2010) use
424 seawater bicarbonate to build their shells (e.g., McConnaughey and Gillikin, 2008). The early non-
425 ferroan micritic to microsparry calcites in the KCM deposits represent the first seep-related cement
426 phase (m1), which locked up the original sediment porosity, and caused later seep fluid to be
427 channelled into conduits (the pipe-like structures). Within these conduits multiple phases of
428 cementation occurred, dominated by the banded and botryoidal fibrous calcite cements (bbc), a
429 common constituent of many modern (e.g. Feng et al., 2010) and ancient seep limestones (e.g. Savard
430 et al., 1996). Based on comparison with other ancient seep limestones (Buggisch and Krumm, 2005;

431 Peckmann et al., 2007a), it seems likely that the primary mineralogy of this phase was aragonite. The
432 overgrowth of faecal pellets by these cements confirms that they had an early diagenetic, pre-
433 compactional origin within the system. The early micrite and fibrous calcite cements from Thyasira
434 Hill have negative $\delta^{13}\text{C}$ values, but are not as low as many other Palaeozoic, Mesozoic, Cenozoic and
435 modern seep carbonate cements (Campbell et al., 2002; Birgel et al., 2006a; Himmler et al., 2008;
436 Haas et al., 2010), and may indicate a greater contribution of thermogenic over biogenic methane in
437 the seep fluids and/or greater admixture of seawater bicarbonate. The former hypothesis has some
438 support from the biomarker results, because the PMI in the bulk sample from Thyasira Hill has only a
439 moderate ^{13}C -depletion (-83%) unlike PMI in other ancient seep carbonates (Birgel et al., 2006a;
440 Kiel et al., 2013), and may be explained by methanotrophic archaea taking up thermogenic methane
441 rather than biogenic methane, which is more ^{13}C -depleted than the former (cf. Whiticar 1999). This
442 has also been suggested for other ancient seep carbonates (e.g. Kaim et al., 2013).

443 The presumed ankerite cements intergrown with the fibrous cements in the KCM fluid
444 conduits represent periodic carbonate precipitation from fluids enriched in Fe and Mn. In general
445 ankerite is rare in seep limestones and only few ancient and modern occurrences have been reported
446 (Peckmann et al., 2001; Díaz-del-Río et al., 2003). The sparry ferroan calcite (ec) and microcrystalline
447 calcite cements (m2) in some of the conduits represent late stage burial cements of uncertain age,
448 probably not derived from hydrocarbons, which filled up any remaining porosity in the conduits
449 centres and elsewhere in the deposits.

450 Some of the molecular fossils in sample Sn1-1 are indicative of micro-organisms involved in
451 AOM. Those indicative of methanotrophic archaea are the isoprenoids PMI, biphytane, and crocetane,
452 as well as the biphytanic diacids. The mixed crocetane/phytane peak (-61%) is less ^{13}C -depleted than
453 PMI, which can be explained by variable precursors of phytane including (1) phototrophic organisms
454 (chlorophyll; e.g. Peters et al., 2005 and references therein) and (2) methanotrophic archaea (archaeol;
455 Peckmann and Thiel, 2004 for a review). Biphytane and biphytanic diacids cannot be used with
456 certainty as AOM biomarkers in this study, since no $\delta^{13}\text{C}$ values are available for these compounds.
457 However, the distribution of biphytanic diacids with 0 to 2 cyclopentane rings resembles the findings

458 in other seep carbonates, where $\delta^{13}\text{C}$ values were available (Birgel et al., 2008a). Therefore, the
459 biphytanic diacids in sample Sn1-1 were likely also sourced by methanotrophic archaea. Biomarkers
460 for SRB involved in AOM are terminally branched fatty acids, especially iso- and anteiso- C_{15} FAs.
461 Usually, anteiso- C_{15} FA predominates over iso- C_{15} FA in *Desulfosarcina* and *Desulfobulbus*, which
462 are the partners of methanotrophic archaea in the three known AOM consortia ANME-1, -2, and -3,
463 respectively (Niemann and Elvert, 2008; Rossel et al., 2011). Interestingly, in case of the SHI seep
464 sample iso- C_{15} FA predominates over anteiso- C_{15} FA and resembles SRB signatures from non-seep
465 microbialites (e.g. Heindel et al., 2012). The strongest ^{13}C -depletion, though, was observed for
466 anteiso- C_{15} FA (-57‰), whereas the other terminally-branched FAs are less ^{13}C -depleted (av. -39‰).
467 This offset most likely points to additional input from other SRB not involved in AOM. Based on the
468 biomarker pattern of the SHI seep sample, the utility of terminally-branched fatty acids as long-lasting
469 molecular fossils of SRB involved in AOM is confirmed for rocks of low to moderate maturity (cf.
470 Birgel et al., 2006a). In the analysed sample, terrigenous organic material is less abundant than marine
471 lipids including short-chain n-alkanes and n-fatty acids. Even though less abundant, the presence of n-
472 C_{27} alkane and n- C_{28} fatty acids still indicates moderate input of terrigenous compounds, most likely
473 derived from leaf waxes, agreeing with the carbon isotopic signatures characteristic of land-derived
474 biomass (-27‰ and -29‰ , respectively). Similar isotopic values from α,ω -diacids have been
475 recorded from the Jurassic Beauvoisin seep deposit (Peckmann and Thiel, 2004), and on the basis of
476 compound-specific $\delta^{13}\text{C}$ values from these compounds it had been concluded that the source biota
477 were not related to AOM. Further, α,ω -diacids with 22 to 24 carbons were suggested to derive from
478 land plants (cf. Pearson et al., 2005, and discussion therein). The presence of land-derived biomass in
479 the KCM is entirely consistent with the shallow water depositional environment and the presence of
480 wood in the seep carbonates (section 2.1).

481

482 5.2. Hydrocarbon seepage on Seymour Island

483 Our interpretation of hydrocarbon seepage in the LBF rests on our analyses of the carbonate-
484 cemented concretions at locality D5.345.2 and the carbonate cements in the articulated '*Thyasira*'

485 townsendi and '*Lucina*' scotti specimens (Table 1). These cements are petrographically similar to
486 those of the SHI deposits, but the $\delta^{13}\text{C}$ values are considerably lower, which for the values as low as
487 -60‰ indicates a contribution of biogenic methane to their formation (cf. Whiticar 1999; Peckmann
488 and Thiel, 2004). As for the SHI deposits, the presence of abundant fibrous, banded and botryoidal
489 cement in the LBF concretions agrees with carbonate formation at seeps. The observed sequence of a
490 yellow variety of this phase predating a translucent variety mirrors paragenetic sequences of other
491 ancient and modern seep limestones (Peckmann et al., 2002; Himmler et al., 2010). The morphology
492 of many of the carbonate-cemented concretions is reminiscent of trace fossils, such as *Thalassinoides*,
493 so we suggest that they represent animal burrows that acted as preferential pathways for the upward
494 flow of fluids in the sediment, and thus acted as loci for the precipitation of seep carbonate cements
495 (e.g. Peckmann et al., 2002). Similar burrow-fills have been observed in both modern (Fig. 5I; Haas et
496 al., 2010; Wetzel, 2013) and ancient (Campbell, 1992; Peckmann et al., 2007b; Mazumdar et al. 2009)
497 hydrocarbon seep sites, sometimes in the periphery of more active areas of seepage (e.g., Jenkins et
498 al., 2007). The absence of large-scale seep deposits on SI we interpret as being a consequence of
499 change in the nature of hydrocarbon flux and source in the James Ross Basin during the Maastrichtian
500 (see section 6.1).

501 The discontinuous layers of '*T.*' townsendi, '*L.*' scotti and *Solemya rossiana* in the LBF on SI
502 could also indicate times of periodic diffuse seepage, as these taxa are putatively chemosymbiotic (see
503 section 5.3) and have congeners that are found at both modern and ancient seep sites (e.g., Kiel
504 2010b). However, at least at genus level, these taxa are not restricted to this environment, commonly
505 occurring in other organic-rich sediments where there are strong redox zones (e.g. seagrass beds and
506 sewage outfalls; e.g. Taylor and Glover, 2006; Taylor et al., 2008; Dando and Southward, 1986), so
507 their presence cannot be used alone as proof of hydrocarbon seepage in the Maastrichtian sediments.

508

509 5.3. Palaeoecology and taxonomic notes

510 The high degree of articulation amongst the specimens of '*Thyasira*' townsendi, '*Lucina*'
511 scotti and *Solemya rossiana* in the KCM and LBF, and the ventral surface-down orientation of many

512 of them shows that they are preserved mostly in-situ and, and have thus not been reworked. This may
513 be surprising, given the shallow water environment in which they lived (see section 2.1), although
514 they were all infaunal taxa and were likely often entombed in sediments by early seep carbonate
515 cementation. All three bivalve taxa belong to families within which either all (Solemyidae and
516 Lucinidae), or some (Thyasiridae), of the living species have symbiotic sulphide-oxidizing bacteria in
517 their gills (Fisher and Childress, 1986; Dando and Southward, 1986; Dando et al., 1986). In the case
518 of the thyasirids, it is the larger species (including the genus *Conchocele*) that have chemosymbionts
519 (Dufour, 2005). Thus, we suggest that '*Thyasira*' townsendi, '*Lucina*' scotti and *Solemya rossiana*
520 had symbionts too, and the association of these species with the seep carbonates in the KCM and LBF
521 is no co-incidence, but indicates the presence of AOM-derived hydrogen sulphide in the Maastrichtian
522 sediments in the basin. However, the presence of a diversity of 'background' benthic molluscan fauna,
523 both epi- and infauna, associated with the chemosymbiotic taxa in the LBF indicates that
524 environmental conditions in the sediment were not too challenging.

525 The ammonites associated with the bivalves in the seep deposits in the KCM we think were
526 most likely not members of the seep communities, although we note that Landman et al. (2012) found
527 isotopically light carbon ($\delta^{13}\text{C}$ values as low as -13.71‰) in the shells of ammonites from one of the
528 Upper Cretaceous (Campanian) Tepee Buttes seep deposits, which they suggest shows ammonites
529 were functionally part of seep communities in the past, at least at this site.

530 '*Thyasira*' townsendi specimens from SHI were first described by Weller (1903) and were
531 identified by him as being conspecific with White's (1890) species *Lucina?* townsendi from
532 Cretaceous sediments on St. Paul's and St. Peter's Islands in the Magellan Strait. Wilckens (1910)
533 later suggested that *Lucina?* townsendi White 1890 is not a lucinid and transferred the species to the
534 genus *Thyasira*. However, as noted by Zinsmeister and Macellari (1988) the shell of '*Thyasira*'
535 townsendi is much larger than those of other *Thyasira* species, and in size and shape more resembles
536 species belonging to *Conchocele* (Kamenev et al., 2001; Okutani, 2002; Oliver and Sellanes, 2005),
537 hence our placement of the genus name '*Thyasira*' in quotation marks herein. Similarly, the shell
538 morphology of '*Lucina*' scotti (Wilckens) 1910 does not correspond well to this genus (or to

539 Wilckens' original genus *Phacoides*) and instead the species very likely belongs to the extinct lucinid
540 genus *Nymphalucina* Speden 1970 (Kiel, 2013), that is particularly well known from seeps and shales
541 in the Western Interior Seaway in North America (Speden, 1970; Kauffman, 1996; Kiel, 2013),
542 because of the external characters (Fig. 5J), and the shape of the cardinal teeth that can be seen in
543 some weathered articulated specimens. Further systematic work is planned on these taxa to
544 substantiate these observations.

545

546 **6. Discussion**

547 6.1. Seepage within the James Ross Basin

548 Our evidence shows that hydrocarbon seepage occurred in the James Ross Basin for a
549 significant period of time during the early to late Maastrichtian. In the early Maastrichtian, during the
550 deposition of the KCM in the present day area Spath Peninsula on SHI, the seepage was apparently
551 more intense and of longer duration, leading to the formation of large carbonate-cemented deposits.
552 The seeping fluids at this time appear to have contained a higher proportion of thermogenic methane
553 over other hydrocarbons, as indicated by the molecular fossil inventory and their compound-specific
554 isotopes in the SHI analysed sample (see section 5.1). By the late Maastrichtian, during the deposition
555 of the LBF on SI, seepage was possibly reduced and occurred only periodically, allowing the
556 formation of communities of chemosymbiotic bivalves and with, at one horizon, carbonated-cemented
557 burrows, but not of large seep deposits. These seep fluids probably had a larger contribution of
558 biogenic methane.

559 There is additional evidence for hydrocarbon seepage at other times and elsewhere in the
560 James Ross Basin area. There are unstudied deposits in the HCM on the Spath Peninsula on SHI and
561 Cape Lamas on SI (Fig. 1) that look similar to those in the KCM, also weathering out from the
562 enclosing sediments, and could thus well be additional seep deposits. Further, stable isotopic studies
563 of calcite cemented concretions from sediments of the Santa Marta Formation (Santonian to
564 Campanian) from northern James Ross Island (Pirrie and Marshall, 1991) and the Maastrichtian aged
565 Sandwich Bluff Member on Vega Island (Pirrie et al., 1994) found a sub-group of concretions

566 preferentially forming within Planolites and Thalassinoides burrow networks with $\delta^{13}\text{C}$ values of
567 -30.4 to -39.2‰ ($n=3$). They interpreted these values to reflect carbon sourced from sulphate
568 reduction and/or methane oxidation (Pirrie and Marshall, 1991). High Mg calcite fibrous fringing
569 cements also occur within the Eocene La Meseta Formation sediments on SI where they infill
570 Teredolites borings in fossil wood (Pirrie et al., 1998). The $\delta^{13}\text{C}$ values of these cements varied
571 between 1.7 and -42.6‰ , although most values were between -10 and -40‰ . Pirrie et al. (1998)
572 interpreted the carbon source for these cements as coming from methane oxidation.

573 Thus, hydrocarbon seepage may have occurred within James Ross Basin from the early
574 Maastrichtian through to the Eocene. The source of the hydrocarbons probably varied over this time
575 period, with biogenic methane being derived from the degradation of organic material, including of
576 terrigenous origin (section 5.1) in shallow sediments, and thermogenic methane forming deeper in the
577 sediment pile during intrusion of the arc-related igneous rocks and making its way to the surface by
578 diffusion, or possibly via faults within the basin, for which, however, there is little evidence at
579 outcrop.

580

581 6.2. Maastrichtian seeps: macroevolutionary considerations

582 The James Ross Basin is only the third published area of Maastrichtian hydrocarbon seepage
583 (the others being the slightly older Tepee Buttes from the Western Interior Basin, USA, and
584 potentially the poorly dated Sada Limestone from Japan). Compared to most other ancient and
585 modern seep communities, the seep fauna of the James Ross Basin is of very low diversity, being
586 dominated by one species (*Thyasira townsendi*), together with smaller numbers of *Solemya rossiana*
587 and (on SI) *Lucina scotti*, all of which probably had thiotrophic chemosymbionts. At present it
588 seems unlikely that any these three taxa were seep obligates, because both *L. scotti* (commonly) and
589 *S. rossiana* (rarely) occur throughout the LBF (Zinsmeister and Macellari, 1988), and the type
590 location of *T. townsendi* on the St. Paul's and St. Peter's Islands has not, to our knowledge, been
591 investigated for the presence of seeps. It is worth noting here that large thyasirid bivalves with very
592 similar morphologies to *T. townsendi* are found in other Cretaceous deposits in the high Southern

593 latitudes, including specimens from Deception Island, Antarctica (Figure 5I) and the species *T.*
594 *bullpointensis* (Stilwell 1994) from North Island, New Zealand.

595 Absent from the James Ross Basin seep fauna are ‘typical’ obligate seep taxa from the
596 Cretaceous (e.g. *Paskentana*, hokkaidoconchids, *Peregrinella*, and *Caspiconcha*), and the Cenozoic
597 (e.g. vesicomysids and bathymodiolins). There are a number of possible explanations for this
598 observation. The first relates to evolutionary history of the obligate seep taxa. The oldest discovered
599 vesicomysids and bathymodiolins are Eocene in age (Amano and Kiel, 2007; Kiel and Amano, 2013),
600 whilst the youngest known representatives of *Paskentana*, *Peregrinella* and *Caspiconcha* are from the
601 Hauterivian (*Paskentana* and *Peregrinella*), and Campanian (*Caspiconcha*) (Campbell and Bottjer,
602 1995; Kiel et al., 2008; Kaim et al., 2008; Jenkins et al., 2013). Thus, the James Ross Basin seep
603 fauna may be both too young to contain representatives of the obligate Mesozoic seep taxa and too old
604 to contain those from the Cenozoic. However, it is worth pointing out here that quite a few obligate
605 seep taxa that ranged from the Cretaceous into the Eocene and younger (such as the gastropods
606 *Ascheria*, *Provanna*, *Desbruyeresia*, *Humptulipsia*, *Retiskenea*, *Serradonta* and *Bathyacmaea*; e.g.
607 Kaim et al., 2014), are all missing from the James Ross Basin seeps.

608 The second possible explanation is palaeolatitudinal. Perhaps Cretaceous high latitude seep
609 faunas were different from contemporary low latitude faunas, as is the case for non-seep communities
610 (Raup and Jablonski, 1993). Negating this hypothesis is that some typical obligate seep taxa are
611 known from high latitude seep sites, both modern and fossil. Examples are the vesicomysids from
612 modern Larsen B seep sites (Domack et al., 2005), hokkaidoconchids from the Late Jurassic
613 Alexander Island seep (Kaim and Kelly, 2009) and *Caspiconcha* from the Lower Cretaceous
614 Greenland seeps (Kelly et al., 2000). The third possible explanation is related to bathymetry. Modern
615 seeps <200 m do not contain obligate taxa (Sahling et al., 2003), and Kiel (2010a) found the same
616 bathymetric control in Cenozoic and Mesozoic seep faunas. Lucinids, thyasirids and solemyids occur
617 in both shallow and deep seep communities, both modern and ancient (e.g. Dando, 2010; Majima et
618 al., 2005; Kiel et al., 2012), so the occurrence of these taxa in James Ross Basin seeps and the absence
619 of any typical seep obligate fauna may have been related solely to the fact that the James Ross Basin

620 seeps occurred in a shallow shelf setting, most probably shallower than 200 metres. Other similar
621 shallow water fossil examples are the Late Cretaceous Teepee Buttes seeps, the core facies of which
622 are dominated by *Nymphalucina occidentalis* (although the total fauna are considerably more diverse
623 than the James Ross Basin seep fauna; Kiel et al., 2012, Kaufmann et al., 1996), the Eocene to
624 Holocene Type III seeps of Majima et al. (2005) from Japan (those dominated by *Lucinoma* and/or
625 *Conchocele* and characterised by autochthonous occurrences in muddy sediments from depths of less
626 than 300 m), and the large lucinids (genus *Monitilora*?) from Late Miocene seeps from Taiwan (Chien
627 et al., 2012).

628 A fourth possible explanation for the absence in the James Ross Basin seeps of ‘typical’
629 Cretaceous obligate seep taxa is ecological. Perhaps seepage in the basin was never vigorous enough
630 for sulphide to reach the seafloor, preventing the settlement of obligate epifauna, such as the
631 gastropod taxa listed above, but still supporting infaunal chemosymbiotic bivalve taxa.

632

633 **Acknowledgments**

634 DB and JP would like to thank Enno Schefuß and Xavier Prieto at the MARUM in Bremen for their
635 help in compound-specific carbon isotope measurements. SK thanks Greg Dietl and Judith Nagel-
636 Myers (Ithaca, NY) for access to the PRI collection and their hospitality during his visit to the PRI.
637 CTSL thanks Laura Tilley for identifying fossil wood fragments in the SHI seep thin sections. JDW
638 thanks James Crampton and Alan Beu (GNS Science, Wellington, New Zealand) for useful discussion
639 and access to fossil collections in their care. Simon Lomas collected some of the material from Snow
640 Hill Island while employed at BAS. We thank Andrzej Kaim and an anonymous reviewer for
641 suggesting improvements to the original version of this paper.

642

643 **References**

644 Agirrezabala, L.M., Kiel, S., Blumenberg, M., Schäfer, N., Reitner, J., 2013. Outcrop analogues of
645 pockmarks and associated methane-seep carbonates: a case study from Lower Cretaceous

- 646 (Albian) of the Basque-Cantabrian Basin, western Pyrenees. *Palaeogeography,*
647 *Palaeoclimatology, Palaeoecology* 390, 94–115.
- 648 Aloisi, G., Pierre, C., Rouchy, J.-M., Foucher, J.-P., Woodside, J., 2000. Methane-related authigenic
649 carbonates of eastern Mediterranean Sea mud volcanoes and their possible relation to gas
650 hydrate destabilization. *Earth and Planetary Science Letters* 184, 321–338.
- 651 Amano, K., Kiel, S., 2007. Fossil vesicomid bivalves from the North Pacific region. *The Veliger* 49,
652 270–293.
- 653 Amano, K., Jenkins, R.G., Aikawa, M., Nobuhara, T., 2010. A Miocene chemosynthetic community
654 from the Ogaya Formation in Joetsu: evidence for depth-related ecologic control among fossil
655 seep communities in the Japan Sea back-arc basin. *Palaeogeography, Palaeoclimatology,*
656 *Palaeoecology* 286, 164–170.
- 657 Baco, A.R., Rowden, A.A., Levin, L.A., Smith, C.R., Bowden, D.A., 2010. Initial characterization of
658 cold seep faunal communities on the New Zealand Hikurangi margin. *Marine Geology* 272,
659 251–259.
- 660 Birgel, D., Peckmann, J., Klautzsch, S., Thiel, V., Reitner, J., 2006a. Anaerobic and aerobic oxidation
661 of methane at Late Cretaceous seeps in the Western Interior Seaway, USA. *Geomicrobiology*
662 *Journal* 23, 565–577.
- 663 Birgel, D., Thiel, V., Hinrichs, K.-U., Elvert, M., Campbell, K. A., Reitner, J., Farmer, J. D.,
664 Peckmann J., 2006b. Lipid biomarker patterns of methane-seep microbialites from the
665 Mesozoic convergent margin of California. *Organic Geochemistry* 37, 1289–1302.
- 666 Birgel, D., Elvert, M., Han, X., Peckmann, J., 2008a. ¹³C-depleted biphytanic diacids as tracers of past
667 anaerobic oxidation of methane. *Organic Geochemistry* 39, 152–156.
- 668 Birgel, D., Himmler, T., Freiwald, A., Peckmann, J., 2008b. A new constraint on the antiquity of
669 anaerobic oxidation of methane: Late Pennsylvanian seep limestones from southern Namibia.
670 *Geology* 36, 543–546.

- 671 Boetius, A., Ravensschlag, K., Schubert, C.J., Rickert, D., Widdel, F., Gieseke, A., Amann, R.,
672 Jørgensen, B.B., Witte, U., Pfannkuche, O., 2000. A marine microbial consortium apparently
673 mediating anaerobic oxidation of methane. *Nature* 407, 623–626.
- 674 Bouloubassi, I., Aloisi, G., Pancost, R., Hopmans, E., Pierre, C., Sinninghe Damsté, J.S., 2006.
675 Archaeal and bacterial lipids in authigenic carbonate crusts from eastern Mediterranean mud
676 volcanoes. *Organic Geochemistry* 37, 484–500.
- 677 Bowman, V.C., Francis, J.E., Riding, J.B., Hunter, S.J., Haywood, A.M., 2012. A latest Cretaceous to
678 earliest Paleogene dinoflagellate cyst zonation from Antarctica, and implications for
679 phytoprovincialism in the high southern latitudes. *Review of Palaeobotany and Palynology*
680 171, 40–56.
- 681 Bowman, V.C., Francis, J.E., Riding, J.B. 2013. Late Cretaceous winter sea ice in Antarctica?
682 *Geology* 41, 1227–1230.
- 683 Buggisch, W., Krumm, S., 2005. Palaeozoic cold seep carbonates from Europe and North Africa – an
684 integrated isotopic and geochemical approach. *Facies* 51, 566–583.
- 685 Campbell, K.A., 1992. Recognition of a Mio-Pliocene cold seep from the northeast Pacific convergent
686 margin, Washington, U.S.A. *Palaios* 7, 422–433.
- 687 Campbell, K.A., 2006. Hydrocarbon seep and hydrothermal vent paleoenvironments and paleontology:
688 past developments and future research directions. *Palaeogeography, Palaeoclimatology,*
689 *Palaeoecology* 232, 362–407.
- 690 Campbell, K.A., Bottjer, D.J., 1995. *Peregrinella*: an Early Cretaceous cold-seep restricted
691 brachiopod. *Paleobiology* 21, 461–478.
- 692 Campbell, K.A, Farmer, J.D., Des Marais, D., 2002. Ancient hydrocarbon seeps from the Mesozoic
693 convergent margin of California: carbonate geochemistry, fluids and palaeoenvironments.
694 *Geofluids* 2, 63–94.
- 695 Charrier, R., Lahsen, A., 1968. Stratigraphy of Late Cretaceous-Early Eocene, Seno Skyring-Strait of
696 Magellan Area, Magallanes Province, Chile. *The American Association of Petroleum*
697 *Geologists Bulletin* 53, 568–590.

- 698 Chien, C.W., Huang, C.Y., Chen, Z., Lee, H.C., Harris, R. 2012. Miocene shallow-marine cold seep
699 carbonate in fold-and-thrust Western Foothills, SW Taiwan. *Journal of Asian Earth Sciences*
700 56, 200–211.
- 701 Cordes, E.E., Carney, S.L., Hourdez, S., Carney, R.S., Brooks, J.M., Fisher, C.R., 2007. Cold seeps of
702 the deep Gulf of Mexico: community structure and biogeographic comparisons to Atlantic
703 equatorial belt seep communities. *Deep-Sea Research I* 54, 637–653.
- 704 Craig, H., 1957. Isotopic standards and isotopic correction factors for mass spectrometric analysis of
705 carbon dioxide. *Geochimica Cosmochimica Acta* 12, 133–149.
- 706 Crame, J.A., Francis, J.E., Cantrill, D.J., Pirrie, D., 2004. Maastrichtian stratigraphy of Antarctica.
707 *Cretaceous Research* 25, 411–423.
- 708 Crame, J.A., Lomas, S.A., Pirrie, D., Luther, A., 1996. Late Cretaceous extinction patterns in
709 Antarctica. *Journal of the Geological Society of London* 153, 503–506.
- 710 Crame, J.A., Luther, A., 1997. The last inoceramid bivalves in Antarctica. *Cretaceous Research* 18,
711 179–195.
- 712 Crame, J.A., McArthur, J.M., Pirrie, D., Riding, J.B., 1999. Strontium isotope correlation of the basal
713 Maastrichtian stage in Antarctica to the European and US biostratigraphic schemes. *Journal of*
714 *the Geological Society of London* 156, 957–964.
- 715 Dando, P.R., 2010. Biological communities at marine shallow-water seep and vent sites. In: S. Kiel
716 (Editor), *The Vent and Seep Biota. Topics in Geobiology*. Springer, Heidelberg, pp. 333–378.
- 717 Dando, P.R., Southward, A.J., 1986. Chemoautotrophy in bivalve molluscs of the genus *Thyasira*.
718 *Journal of the Marine Biological Association of the U.K.* 66, 915–929.
- 719 Dando, P.R., Southward, A.J., Southward, E.C., 1986. Chemoautotrophic symbionts in the gills of the
720 bivalve mollusc *Lucinoma borealis* and the sediment chemistry of its habitat. *Proceedings of*
721 *the Royal Society of London, B* 227, 227–247.
- 722 Díaz-del-Río, V., Somoza, L., Martínez-Frias, J., Mata, M.P., Delgado, A., Hernandez-Molina, F.J.,
723 Lunar, R., Martín-Rubí, J.A., Maestro, A., Fernández-Puga, M.C., León, R., Llave, E.
724 Medialdea, T., Vázquez, J.T., 2003. Vast fields of hydrocarbon-derived carbonate chimneys

- 725 related to the accretionary wedge/olistostrome of the Gulf of Cádiz. *Marine Geology* 195,
726 177–200.
- 727 Dingle, R.V., 1995. Report of fieldwork undertaken in the Snow Hill Island-James Ross Island area
728 and around Low Head, King George Island: December 1994-February 1995. British Antarctic
729 Survey unpublished field report, R/1994/GL1.
- 730 Domack, E., Ishman, S., Leventer, A., Sylva, S., Willmott, V., Huber, B., 2005. A chemotrophic
731 ecosystem found beneath Antarctic ice shelf. *Eos*, 86, 269–276.
- 732 Dubilier, N., Bergin, C., Lott, C., 2008. Symbiotic diversity in marine animals: the art of harnessing
733 chemosynthesis. *Nature Reviews Microbiology* 6, 725–740.
- 734 Dufour, S.C., 2005. Gill anatomy and the evolution of symbiosis in the bivalve family Thyasiridae.
735 *Biological Bulletin* 208, 200–212.
- 736 Dutton, A., Huber, B.T., Lohmann, K. C., Zinsmeister, W.J., 2007. High-resolution stable isotope
737 profiles of a dimitobelid belemnite: implications for paleodepth habitat and late Maastrichtian
738 climate seasonality. *Palaios* 22, 642-650.
- 739 Elvert, M., Greinert, J., Suess, E., Whiticar, M.J., 2000. Archaea mediating anaerobic methane
740 oxidation in deep-sea sediments at cold seeps of the eastern Aleutian subduction zone.
741 *Organic Geochemistry* 31, 1175–1187.
- 742 Feng, D., Chen, D., Peckmann, J., Bohrmann, G., 2010. Authigenic carbonates from methane seeps of
743 the northern Congo fan: Microbial formation mechanism. *Marine and Petroleum Geology* 27,
744 748–756.
- 745 Fisher, C.R., Childress, J.J., 1986. Translocation of fixed carbon from symbiotic bacteria to host
746 tissues in the gutless bivalve *Solemya reidi*. *Marine Biology* 93, 59–68.
- 747 Friedrich, O., Norris, R.D., Erbacher, J., 2012. Evolution of middle to Late Cretaceous oceans – A 55
748 m.y. record of Earth’s temperature and carbon cycle. *Geology* 40, 107–110.
- 749 Gardin, S., Galbrun, B., Thibault, N., Coccioni, R., Premoli-Silva, I., 2012. Bio-magnetostratigraphy
750 for the upper Campanian - Maastrichtian from the Gubbio area, Italy: new results from the
751 Contessa Highway and Bottaccione sections. *Newsletters on Stratigraphy* 45, 75–103.

- 752 Goedert, J.L., Squires, R.L., 1990. Eocene deep-sea communities in localized limestones formed by
753 subduction-related methane seeps, southwestern Washington. *Geology* 18, 1182–1185.
- 754 Haas, A., Peckmann, J., Elvert, M., Sahling, H., Bohrmann, G., 2010. Patterns of carbonate
755 authigenesis at the Kouilou pockmarks on the Congo deep-sea fan. *Marine Geology* 268,
756 129–136.
- 757 Han, X., Suess, E., Sahling, H., Wallmann, K., 2004. Fluid venting activity on the Costa Rica margin:
758 new results from authigenic carbonates. *International Journal of Earth Sciences* 93, 596–611.
- 759 Heindel, K., Birgel, D., Brunner, B., Thiel, V., Westphal, H., Gischler, E., Ziegenbalg, S.B., Cabioch,
760 G., Sjövall, P., Peckmann, J., 2012. Post-glacial microbialite formation in coral reefs of the
761 Pacific, Atlantic, and Indian Oceans. *Chemical Geology* 304–305, 117–130.
- 762 Henderson, R.A., 1970. Ammonoidea from the Mata Series (Santonian – Maastrichtian) of New
763 Zealand. *Special Papers in Palaeontology* 6, 82p.
- 764 Henderson, R.A., McNamara, K.J., 1985. Maastrichtian non-heteromorph ammonites from the Miria
765 Formation, Western Australia. *Palaeontology* 28, 35–88.
- 766 Himmler, T., Bach, W., Bohrmann, G., Peckmann, J., 2010. Rare earth elements in authigenic
767 methane-seep carbonates as tracers for fluid composition during early diagenesis. *Chemical*
768 *Geology* 277, 126–136.
- 769 Himmler, T., Freiwald, A., Stollhofen, H., Peckmann, J., 2008. Late Carboniferous hydrocarbon-seep
770 carbonates from the glaciomarine Dwyka Group, southern Namibia. *Palaeogeography,*
771 *Palaeoclimatology, Palaeoecology* 257, 185–197.
- 772 Hinrichs, K.-U., Hayes, J.M., Sylva, S.P., Brewer, P.G., DeLong, E.F., 1999. Methane-consuming
773 archaeobacteria in marine sediments. *Nature* 398, 802–805.
- 774 Husson, D., Galbrun, B., Laskar, J., Hinnov, L., Thibault, N., Gardin, S., Locklair, R.E., 2011.
775 Astronomical calibration of the Maastrichtian (late Cretaceous). *Earth and Planetary Science*
776 *Letters* 305, 328–340.

- 777 Jenkins, R.G., Kaim, A., Little, C.T.S., Iba, Y., Tanabe, K., Campbell, K.A., 2013. Worldwide
778 distribution of modiomorphid bivalve genus *Caspiconcha* in late Mesozoic hydrocarbon
779 seeps. *Acta Palaeontologica Polonica* 58, 357–382.
- 780 Jenkins, R.G., Kaim, A., Hikida, Y., Tanabe, K., 2007. Methane-flux-dependent lateral faunal
781 changes in a Late Cretaceous chemosymbiotic assemblage from the Nakagawa area of
782 Hokkaido, Japan. *Geobiology* 5, 127–139.
- 783 Judd, A., Hovland, M., 2009. *Seabed Fluid Flow*. Cambridge University Press. 492 pp.
- 784 Kaim, A., Kelly, S.R.A., 2009. Mass occurrence of hokkaidoconchid gastropods in the Upper Jurassic
785 methane seep carbonate from Alexander Island, Antarctica. *Antarctic Science* 21, 279–284.
- 786 Kaim, A., Jenkins, R.G., Warén, A., 2008. Provannid and provannid-like gastropods from the Late
787 Cretaceous cold seeps of Hokkaido (Japan) and the fossil record of the Provannidae
788 (Gastropoda: Abysochrysoidea). *Zoological Journal of the Linnean Society* 154, 421–436.
- 789 Kaim, A., Skupien, P., Jenkins, R.G., 2013. A new Lower Cretaceous hydrocarbon seep locality from
790 the Czech Carpathians and its fauna. *Palaeogeography, Palaeoclimatology, Palaeoecology*
791 390, 42–51. Kaim, A., Jenkins, R.G., Tanabe, K., Kiel, S., 2014. Mollusks from late Mesozoic
792 seep deposits, chiefly in California. *Zootaxa* 3861, 401–440.
- 793 Kamenev, G.M., Nadtochy, V.A., Kuznetsov, A.P., 2001. *Conchocele bisecta* (Conrad, 1849)
794 (Bivalvia: Thyasiridae) from cold-water methane-rich areas of the Sea of Okhotsk. *The*
795 *Veliger* 44, 84–94.
- 796 Kauffman, E.G., Arthur, M.A., Howe, B., Scholle, P.A., 1996. Widespread venting of methane-rich
797 fluids in Late Cretaceous (Campanian) submarine springs (Tepee Buttes), Western Interior
798 seaway, U.S.A. *Geology* 24, 799–802.
- 799 Kelly, S.R.A., Blanc, E., Price, S.P., Witham, A.G., 2000. Early Cretaceous giant bivalves from
800 seep-related limestone mounds, Wollaston Forland, Northeast Greenland. In: Harper, E.M.,
801 Taylor, J.D., Crame, J.A. (Eds.), *The Evolutionary Biology of the Bivalvia: Geological*
802 *Society, London, Special Publications*, 177, pp. 227–246.

- 803 Kennedy, W.J., Crame, J.A., Bengtson, P., Thompson, M.R.A., 2007. Coniacian ammonites from
804 James Ross Island, Antarctica. *Cretaceous Research* 28, 509–531.
- 805 Kennedy, W.J., Klinger, H.C., 1985. Cretaceous faunas from Zululand and Natal, South Africa. The
806 ammonite family Kossmaticeratidae Spath, 1922. *Annals of the South African Museum* 95,
807 165–231.
- 808 Kiel, S., 2010a. On the potential generality of depth-related ecologic structure in cold-seep
809 communities: Evidence from Cenozoic and Mesozoic examples. *Palaeogeography,*
810 *Palaeoclimatology, Palaeoecology* 295, 245–257.
- 811 Kiel, S., 2010b. The fossil record of vent and seep mollusks. In: S. Kiel (Editor), *The Vent and Seep*
812 *Biota. Topics in Geobiology.* Springer, Heidelberg, pp. 255–278.
- 813 Kiel, S., 2013. Lucinid bivalves from ancient methane seeps. *Journal of The Malacological Society of*
814 *London* 79, 346–363.
- 815 Kiel, S., Amano, K., 2013. The earliest bathymodiolin mussels: An evaluation of Eocene and
816 Oligocene taxa from deep-sea methane seep deposits in Western Washington State, USA.
817 *Journal of Paleontology* 87, 589–602.
- 818 Kiel, S., Little, C.T.S., 2006. Cold seep mollusks are older than the general marine mollusk fauna.
819 *Science* 313, 1429–1431.
- 820 Kiel, S., Birgel, D., Campbell, K.A., Crampton, J.S., Schiøler, P., Peckmann, J., 2013. Cretaceous
821 methane-seep deposits from New Zealand and their fauna. *Palaeogeography,*
822 *Palaeoclimatology, Palaeoecology* 390, 17–34.
- 823 Kiel, S., Campbell, K.A., Elder, W.P., Little, C.T.S., 2008. Jurassic and Cretaceous gastropods from
824 hydrocarbon-seeps in forearc basin and accretionary prism settings, California. *Acta*
825 *Palaeontologica Polonica* 53, 679–703.
- 826 Kiel, S., Wiese, F., Titus, A.L., 2012. Shallow-water methane-seep faunas in the Cenomanian
827 Western Interior Seaway: No evidence for onshore-offshore adaptations to deep-sea vents.
828 *Geology* 40, 839–842.

- 829 Landman, N.H., Cochran, J.K., Larson, N.L., Brezina, J., Garb, M.P., Harries, P.J., 2012. Methane
830 seeps as ammonite habitats in the U.S. Western Interior Seaway revealed by isotopic analyses
831 of well-preserved shell material. *Geology* 40, 507–510.
- 832 Lartaud, F., de Rafelis, M., Oliver, G., Krylova, E., Dymont, J., Ildefonse, B., Thibaud, R., Gente, P.,
833 Hoisé, E., Meistertzheim, A.L., Fouquet, Y., Gaill F., Le Bris, N., 2010. Fossil clams from a
834 serpentinite-hosted sedimented vent field near the active smoker complex Rainbow (MAR,
835 26°13N): insight into the biogeography of vent fauna. *Geochemistry Geophysics Geosystems*
836 11, Q0AE01.
- 837 Levin, L.A., 2005. Ecology of cold seep sediments: interactions of fauna with flow, chemistry and
838 microbes. *Oceanography and Marine Biology. Annual Review* 43, 1–46.
- 839 Levin, L.A., James, D.W., Martin, C.M., Rathburn, A.E., Harris, L.H., Michener, R.H., 2000. Do
840 methane seeps support distinct macrofaunal assemblages? Observations on community
841 structure and nutrition from the northern California slope and shelf. *Marine Ecology Progress*
842 *Series* 208, 21–39.
- 843 Lomas, S.A., 1995. Sedimentological and stratigraphic studies of Snow Hill Island, 1994/95. British
844 Antarctic Survey unpublished field report, R/1994/GL5.
- 845 Macellari, C.E., 1986. Late Campanian-Maastrichtian ammonite fauna from Seymour Island
846 (Antarctic Peninsula). *Memoir (The Paleontological Society)* 18, 1–55
- 847 Majima, R., Nobuhara, T., Kitazaki, T., 2005. Review of fossil chemosynthetic assemblages in Japan.
848 *Palaeogeography, Palaeoclimatology, Palaeoecology* 227, 86–123.
- 849 Mazumdar, A., Joshi, R.K., Peketi, A., Kocherla, M., 2011. Occurrence of faecal pellet-filled simple
850 and composite burrows in cold seep carbonates: a glimpse of a complex benthic ecosystem.
851 *Marine Geology* 289, 117–121.
- 852 McArthur, J.M., Thirlwall, M.F., Engkilde, M., Zinsmeister, W.J., Howarth, R.J., 1998. Strontium
853 isotope profiles across K/T boundary sequences in Denmark and Antarctica. *Earth and*
854 *Planetary Science Letters* 160, 179–192.

- 855 McArthur, J.M., Crame, J.A., Thirlwall, J.E., 2000. Definition of Late Cretaceous stage boundaries in
856 Antarctica using strontium isotope stratigraphy *Journal of Geology* 108, 623–640.
- 857 McConnaughey, T.A., Gillikin, D.P., 2008. Carbon isotopes in mollusk shell carbonates, *Geo-Marine*
858 *Letters* 28, 287–299.
- 859 Metz, C.L., 2010. Tectonic controls on the genesis and distribution of Late Cretaceous, Western
860 Interior Basin hydrocarbon-seep mounds (Tepee Buttes) of North America. *Journal of*
861 *Geology* 118, 201–213.
- 862 Naehr, T.H., Eichhubl, P., Orphan, V.J., Hovland, M., Paull, C.K., Ussler III, W., Lorenson, T.D.,
863 Greene, H.G., 2007. Authigenic carbonate formation at hydrocarbon seeps in continental
864 margin sediments: a comparative study. *Deep-Sea Research II* 54, 1268–1291.
- 865 Niemann, H., Elvert, M., 2008. Diagnostic lipid biomarker and stable carbon isotope signatures of
866 microbial communities mediating the anaerobic oxidation of methane with sulphate. *Organic*
867 *Geochemistry* 39, 1668–1677.
- 868 Niemann, H., Fischer, D., Graffe, D., Knittel, K., Montiel, A., Heilmayer, O., Nöthen, K., Pape, T.,
869 Kasten, S., Bohrmann, G., Boetius, A., Gutt, J., 2009. Biogeochemistry of a low-activity cold
870 seep in the Larsen B area, western Weddell Sea, Antarctica. *Biogeosciences* 6, 2383–2395.
- 871 Nobuhara, T., Onda, D., Kikuchi, N., Kondo, Y., Matsubara, K., Amano, K., Jenkins, R.G., Hikida,
872 Y., Majima, R., 2008. Lithofacies and fossil assemblages of the Upper Cretaceous Sada
873 Limestone, Shimanto City, Kochi Prefecture, Shikoku, Japan. *Fossils, The Palaeontological*
874 *Society of Japan* 84, 47–60.
- 875 Okutani, T., 2002. A new thyasirid Conchocele novaeguineensis n. sp. from a thanatocoenosis
876 associated with a possible cold seep activity off New Guinea. *Venus*, 61, 141–145.
- 877 Oliver, P.G., Killeen, I.J., 2002. The Thyasiridae (Mollusca: Bivalvia) of the British continental shelf
878 and North Sea oilfields. An identification manual. *Studies in Marine Biodiversity and*
879 *Systematics from the National Museum of Wales. BIOMÔR Reports* 3, 1–73.
- 880 Oliver, P.G., Sellanes, J., 2005. New species of Thyasiridae from a methane seepage area off
881 Concepción, Chile. *Zootaxa* 1092, 1–20.

- 882 Olivero, E.B., 1984. Nuevos amonites Campanianos de la Isla James Ross, Antartida. *Ameghiniana*
883 21, 53–84.
- 884 Olivero, E.B., 1988. Early Campanian heteromorph ammonites from James Ross Island, Antarctica.
885 *National Geographic Research* 4, 259–271.
- 886 Olivero, E.B., 1992. Asociaciones de Amonites de la Formacion Santa Marta (Cretacico Tardio), Isla
887 James Ross, Antartida. In: C.A. Rinaldi (Ed.), *Geología de la Isla James Ross, Instituto*
888 *Antártico Argentino, Buenos Aires (1992)*, 47–76.
- 889 Olivero, E.B., 2012. Sedimentary cycles, ammonite diversity and palaeoenvironmental changes in the
890 Upper Cretaceous Marambio Group, Antarctica. *Cretaceous Research* 34, 348–366.
- 891 Olivero, E.B., Medina, F.A., 2000. Patterns of Late Cretaceous ammonite biogeography in southern
892 high latitudes: the family Kossmaticeratidae in Antarctica. *Cretaceous Research* 21, 269–279.
- 893 Olivero, E.B., Ponce, J.J., Martinioni, D.R., 2008. Sedimentology and architecture of sharp-based
894 tidal sandstones in the upper Marambio Group, Maastrichtian of Antarctica. *Sedimentary*
895 *Geology* 210, 11–26.
- 896 Paull, C.K., Hecker, B., Commeau, R., Freeman-Lynde, R.P., Neumann, C., Corso, W.P., Golubic, S.,
897 Hook, J.E., Sikes, E., Curray, J., 1984. Biological communities at the Florida Escarpment
898 resemble hydrothermal vent taxa. *Science* 226, 965–967.
- 899 Pearson, M.J., Hendry, J.P., Taylor, C.W., Russell, M.A., 2005. Fatty acids in sparry calcite fracture
900 fills and microsparite cement of septarian diagenetic concretions. *Geochimica et*
901 *Cosmochimica Acta* 69, 1773–1786.
- 902 Peckmann, J., Thiel, V., 2004. Carbon cycling at ancient methane-seeps. *Chemical Geology* 205,
903 443–467.
- 904 Peckmann, J., Campbell, K.A., Walliser, O.H., Reitner, J., 2007a. A Late Devonian hydrocarbon-seep
905 deposit dominated by dimerelloid brachiopods, Morocco. *Palaios* 22, 114–122.
- 906 Peckmann, J., Gischler, E., Oschmann, W., Reitner, J., 2001. An Early Carboniferous seep
907 community and hydrocarbon-derived carbonates from the Harz Mountains, Germany.
908 *Geology* 29, 271–274.

- 909 Peckmann, J., Goedert, J.L., Thiel, V., Michaelis, W., Reitner, J., 2002. A comprehensive approach to
910 the study of methane-seep deposits from the Lincoln Creek Formation, western Washington
911 State, USA. *Sedimentology* 49, 855–873.
- 912 Peckmann, J., Senowbari-Daryan, B., Birgel, D., Goedert, J.L., 2007b. The crustacean ichnofossil
913 *Palaxius* associated with callianassid body fossils in an Eocene methane-seep limestone,
914 Humptulips Formation, Olympic Peninsula, Washington. *Lethaia* 40, 273–280.
- 915 Peckmann, J., Thiel, V., Michaelis, W., Clari, P., Gaillard, C., Martire, L., Reitner, J., 1999. Cold seep
916 deposits of Beauvoisin (Oxfordian, southeastern France) and Marmorito (Miocene, northern
917 Italy): microbially induced authigenic carbonates. *International Journal of Earth Sciences* 88,
918 60–75.
- 919 Peters, K.E., Walters, C.C., Moldowan, J. M., 2005. *The Biomarker Guide*. Cambridge University
920 Press (1155 pp.).
- 921 Pirrie, D., Marshall, J.D., 1990. High paleolatitide Late Cretaceous paleotemperatures: new data from
922 James Ross Island, Antarctica. *Geology* 18, 31–34.
- 923 Pirrie, D., Marshall, J.D., 1991. Field relationships and stable isotope geochemistry of concretions
924 from James Ross Island, Antarctica. *Sedimentary Geology* 71, 137–150.
- 925 Pirrie, D., Ditchfield, P.W., Marshall, J.D., 1994. Burial diagenesis and pore-fluid evolution in a
926 Mesozoic back-arc basin: the Marambio Group, Vega Island, Antarctica. *Journal of*
927 *Sedimentary Research* 64, 541–552.
- 928 Pirrie, D., Crame, J.A., Lomas, S.A., Riding, J.B. 1997. Late Cretaceous stratigraphy of the Admiralty
929 Sound region, James Ross Basin, Antarctica. *Cretaceous Research* 18, 109–137.
- 930 Pirrie, D., Marshall, J.D., Crame, J.A., 1998. Marine high Mg calcite cements in Teredolites-bored
931 fossil wood; evidence for cool paleoclimates in the Eocene La Meseta Formation, Seymour
932 Island, Antarctica. *Palaios* 13, 276–286.
- 933 Pirrie, D., Butcher, A.R., Power, M.R., Gottlieb, P., Miller, G.L., 2004. Rapid quantitative mineral
934 and phase analysis using automated scanning electron microscopy (QemSCAN); potential
935 applications in forensic geoscience. In Pye, K. & Croft, D.J. (eds) *Forensic Geoscience:*

- 936 Principles, Techniques and Applications. Geological Society, London, Special Publication
937 232, 123–136.
- 938 Pirrie, D., Rollinson, G.K., Andersen, J.A., Wootton, D., Moorhead, S., 2014. Soil forensics as a tool
939 to test reported artefact find sites. *Journal of Archaeological Science* 41, 461–473.
- 940 Raup, D.M., Jablonski, D., 1993. Geography of end-Cretaceous marine bivalve extinctions. *Science*
941 260, 971–973.
- 942 Reitner, J., Peckmann, J., Blumenberg, M., Michaelis, W., Reimer, A., Thiel, V., 2005. Concretionary
943 methane-seep carbonates and associated microbial communities in Black Sea sediments.
944 *Palaeogeography, Palaeoclimatology, Palaeoecology* 227, 18–30.
- 945 Ritger, S., Carson, B., Suess, E., 1987. Methane-derived authigenic carbonates formed by subduction-
946 induced pore-water expulsion along the Oregon/Washington margin. *Geological Society of*
947 *America Bulletin* 98, 147–156.
- 948 Rossel, P.E., Elvert, M., Ramette, A., Boetius, A., Hinrichs, K.-U., 2011. Factors controlling the
949 distribution of anaerobic methanotrophic communities in marine environments: Evidence
950 from intact polar membrane lipids. *Geochimica et Cosmochimica Acta* 75, 164–184.
- 951 Sahling, H., Galkin, S.V., Salyuk, A., Greinert, J., Foerstel, H., Piepenburg, D., Suess, E., 2003.
952 Depth-related structure and ecological significance of cold-seep communities – a case study
953 from the Sea of Okhotsk. *Deep-sea Research I* 50, 1391–1409.
- 954 Salazar, C., Stinnesbeck, W., Qunzio-Sinn, L.A., 2010. Ammonites from the Maastrichtian (Upper
955 Cretaceous) Quiriquina Formation in central Chile. *Neues Jahrbuch für Geologie und*
956 *Paläontologie* 257, 181–236.
- 957 Savard, M.M., Beauchamp, B., Veizer, J., 1996. Significance of aragonite cements around Cretaceous
958 marine methane seeps. *Journal of Sedimentary Research* 66, 430–328.
- 959 Schwartz, H., Sample, J., Weberling, K.D., Minisini, D., Moore, J.C., 2003. An ancient linked fluid
960 migration system: Cold-seep deposits and sandstone intrusions in the Panoche Hills,
961 California, USA. *Geo-Marine Letters* 23, 340–350.

- 962 Sellanes, J., Quiroga, E., Gallardo, V.A., 2004. First direct evidence of methane seepage and
963 associated chemosynthetic communities in the bathyal zone off Chile. *Journal of the Marine*
964 *Biological Association of the United Kingdom* 84, 1065–1066.
- 965 Sibuet, M., Olu, K., 1998. Biogeography, biodiversity and fluid dependence of deep-sea cold-seep
966 communities at active and passive margins. *Deep-Sea Research II* 45, 517–567.
- 967 Speden, I.G., 1970. The type Fox Hills Formation, Cretaceous (Maestrichtian), South Dakota. Part 2.
968 Systematics of the Bivalvia. Peabody Museum of Natural History Yale University, *Bulletin*
969 33, 1–222.
- 970 Stilwell, J.D., 1994. Latest Cretaceous to earliest Paleogene molluscan faunas of New Zealand:
971 changes in composition as a consequence of break-up of Gondwana and extinction.
972 Unpublished PhD dissertation, University of Otago, Dunedin, 1630 pp, 84 pls.
- 973 Stinnesbeck, W., Ifrim, C., Salazar, C., 2012. The last Cretaceous ammonites in Latin America. *Acta*
974 *Palaeontologica Polonica* 57, 717–728.
- 975 Taylor, J.D., Glover, E.A., 2006. Lucinidae (Bivalvia) - the most diverse group of chemosymbiotic
976 molluscs. *Zoological Journal of the Linnean Society*, 148, 421–438.
- 977 Taylor, J.D., Glover, E.A., Williams, S.T., 2008. Ancient shallow water chemosynthetic bivalves:
978 systematics of Solemyidae from eastern and southern Australia (Mollusca, Bivalvia).
979 *Memoires of the Queensland Museum – Nature* 54, 75–104.
- 980 Thiel, V., Peckmann, J., Seifert, R., Wehrung, P., Reitner, J., Michaelis, W., 1999. Highly isotopically
981 depleted isoprenoids: molecular markers for ancient methane venting. *Geochimica et*
982 *Cosmochimica Acta* 63, 3959–3966.
- 983 Tobin, T.S., Ward, P.D., Steig, E.J., Olivero, E.B., Hilburn, I.A., Mitchell, R.D., Diamond, M.R.,
984 Raub, T.D., Kirschvink, J.L., 2012. Extinction patterns, $\delta^{18}\text{O}$ trends, and magnetostratigraphy
985 from a southern high-latitude Cretaceous-Paleogene section: Links with Deccan volcanism.
986 *Palaeogeography, Palaeoclimatology, Palaeoecology* 350-352, 180–188.

- 987 Voigt, S., Gale, A.S., Jung, C., Jenkyns, H.C., 2012. Global correlation of Upper Campanian -
988 Maastrichtian successions using carbon-isotope stratigraphy: development of a new
989 Maastrichtian timescale. *Newsletters on Stratigraphy* 45, 25–53.
- 990 Walaszczyk, I., Kennedy, W.J., Klinger, H.C., 2009. Cretaceous faunas from Zululand and Natal,
991 South Africa. Systemic palaeontology and stratigraphical potential of the Upper Campanian-
992 Maastrichtian Inoceramidae (Bivalvia). *African Natural History* 5, 49–132.
- 993 Weller, S., 1903. The Stokes collection of Antarctic fossils. *The Journal of Geology* 11, 413-419.
- 994 Wetzel, A., 2013. Formation of methane-related authigenic carbonates within the bioturbated zone -
995 An example from the upwelling area off Vietnam. *Palaeogeography, Palaeoclimatology,*
996 *Palaeoecology* 386, 23–33.
- 997 Wilckens, O., 1910. Die Anneliden, Bivalven, und Gastropoden der Antarktischen
998 Kreideformationen. *Wissenschaftliche Ergebnisse der Schwedischen Südpolar-Expedition,*
999 *1901–1903* 3, 1–132.
- 1000 White, C.A., 1890. On certain Mesozoic fossils from the Islands of St. Paul's and St. Peter's in the
1001 Straits of Magellan. *Proceedings of the United States National Museum* 13, 13–14.
- 1002 Whiticar, M.J., 1999. Carbon and hydrogen isotope systematics of bacterial formation and oxidation
1003 of methane. *Chemical Geology* 161, 291–314.
- 1004 Zinsmeister, W.J., 1998. Discovery of fish mortality horizon at the K-T boundary on Seymour Island:
1005 Re-evaluation of events at the end of the Cretaceous. *Journal of Paleontology* 72, 556–571.
- 1006 Zinsmeister, W.J., Feldmann, R.M., 1996. Late Cretaceous faunal changes in the high southern
1007 latitudes: a harbinger of global catastrophe? In: McLeod, N., Keller, G. (Eds.), *Biotic and*
1008 *Environmental Events across the Cretaceous/Tertiary Boundary*. Norton, New York, NY,
1009 303–326.
- 1010 Zinsmeister, W.J., Macellari, C.E., 1988. Bivalvia (Mollusca) from Seymour Island, Antarctic
1011 Peninsula. In: Feldmann, R.M., Woodburne, M.O. (Eds.), *Geology and Paleontology of*
1012 *Seymour Island, Antarctic Peninsula*. Geological Society of America Memoirs 169, 253–284.
- 1013
- 1014

1015 **Figure captions**

1016 **Fig. 1.** (A) Locality map showing outcrops of Marambio Group sediments in the Trinity Peninsula
1017 and James Ross Island areas of Antarctica (inset). (B) Outline geological map of Seymour Island and
1018 the NE tip of Snow Hill Island; modified from Crame et al. (2004).

1019
1020 **Fig. 2.** Composite stratigraphy of the Maastrichtian part of the Marambio Group on Snow Hill and
1021 Seymour Islands, following Pirrie et al. (1997), Crame et al. (2004) Bowman et al. (2013) for
1022 lithostratigraphy and biostratigraphy, and MacArthur et al. (1998), Tobin et al. (2012), and Bowman
1023 et al. (2013) for chronostratigraphy. Stars mark the approximate positions of the studied hydrocarbon
1024 seep deposits in the stratigraphic column. Black circles indicate other occurrences of the
1025 chemosynthetic bivalve assemblage ('*Thyasira*', '*Lucina*', *Solemya*) collected during BAS
1026 expeditions. Abbreviations: SHI = Snow Hill Island; KCM = Karlsen Cliffs Member; HCM = Haslum
1027 Crag Member; S = Sobral Formation; K = Cretaceous; Pg = Paleogene; Dan = Danian.

1028
1029 **Fig. 3.** Field images of carbonate cemented sediments and associated fossils from BAS section DJ.616
1030 in the Karlsen Cliffs Member, near Nordenskjold's Hut, Snow Hill Island, looking towards the SW.
1031 The section (A) runs from the base of the hill, bottom right of the photograph, up the slope through
1032 points where photographs (C-E) were taken, over *Thyasira* Hill to BAS locality DJ.617. The cliffs at
1033 the top left of the photograph (A) are outcrops of the Haslum Crag Member. The white arrow points
1034 in the younging direction, perpendicular to the dip of the beds. (B) and (D) Irregularly shaped patches
1035 of carbonate cemented sediments. (C) In-situ articulated '*Thyasira townsendi*' specimens in plan view
1036 on the surface of an exposed bedding plane. (E) Ammonites and articulated '*Thyasira townsendi*
1037 specimens, base of *Thyasira* Hill. Geological hammers for scale in (B) (see white arrow), (C), (D) and
1038 (E) approximately 40 cm long.

1039
1040 **Fig. 4.** Field images of carbonate cemented sediments and associated fossils from Karlsen Cliffs
1041 Member, Snow Hill Island. (A) *Thyasira* Hill; arrow shows position of image (C). (B) Knolls of

1042 exhumed carbonate cemented sediment, approximately 200 m East of Thyasira Hill; arrow shows
 1043 position of image (D). Outcrops in the hills in background are Haslum Crag Member. (C) Detail of
 1044 (A) showing carbonate cemented sediment enclosing weathered articulated '*Thyasira*' townsendi
 1045 specimens; sample Sn1-1 comes from this location. (D) Detail of knoll in (B) with Thyasira Hill in
 1046 background, to left; arrow points to hammer scale. Geological hammers for scale in (C) and (D)
 1047 approximately 30 cm long.

1048

1049 **Fig. 5.** Fossils and carbonate concretions from Snow Hill and Seymour Islands. (A) Hand specimen of
 1050 carbonated cemented siltstone, sample Sn1-1, Thyasira Hill, Karlsen Cliffs Member, Snow Hill
 1051 Island. White arrows point to articulated '*Thyasira*' townsendi specimens in various sections. Black
 1052 arrow points to sparry calcite cement patch. Codes 1A and B are sites where matrix samples (Sn1-1a
 1053 and Sn1-1b respectively) were drilled for stable isotope analysis (see Table 2). This specimen was
 1054 subsequently destroyed for biomarker analysis. (B) Three cut tubular carbonate concretions from
 1055 locality D5.345.2, López de Bertodano Formation, Seymour Island. The concretion on the right hand
 1056 side was sectioned and its exposed centre drilled for stable isotope analysis (sample D5.345.2 a; see
 1057 Table 2). Note the presence of small Planolites-like burrows on the surface of the concretion. (C)
 1058 Carbonate concretion formed of cemented large burrows with smaller burrows on their surfaces; from
 1059 Hydrate Hole seep site, 3100 m water depth, Congo deep-sea fan (see Haas et al., 2010 for details);
 1060 specimen GeoB 8212-1. (D) Ammonite *Maorites seymourianus* from locality D5.347.2, López de
 1061 Bertodano Formation, Seymour Island. (E) Ammonite *Gunnarites* sp., possibly *Gunnarites*
 1062 *bhavaniformis* from locality DJ.633.1, Karlsen Cliffs Member, Snow Hill Island. (F) Ammonite
 1063 *Jacobites anderssoni* from locality DJ.633.1, Karlsen Cliffs Member, Snow Hill Island. (G) Right
 1064 valve of articulated specimen of bivalve '*Thyasira*' townsendi from Thyasira Hill, Snow Hill Island;
 1065 shell material present on umbo and anterior margin. (H) Right valve of articulated specimen of
 1066 bivalve '*Thyasira*' townsendi from locality D5.345.2, López de Bertodano Formation, Seymour
 1067 Island; internal mould. (I) Left valve of articulated large thyasirid bivalve from Deception Island,
 1068 Antarctica; Paleontological Research Institution 1464. (J) Right valve of articulated specimen of

1069 bivalve *'Lucina' scotti*, Paleontological Research Institution 62282, locality PU 1149, López de
 1070 Bertodano Formation, Seymour Island. (K) Right valve of bivalve *Solemya rossiana*, locality
 1071 D5.345.2, López de Bertodano Formation, Seymour Island. All fossils whitened with ammonium
 1072 chloride powder. Scale bars A-C = 10 mm; D-K = 20 mm.

1073

1074 **Fig. 6.** Images of petrographic thin sections from concretionary carbonate from sample DJ.633.3,
 1075 Karlsen Cliffs Member, Snow Hill Island (A, C, D) and carbonate concretion D5.345.2 b1 from
 1076 López de Bertodano Formation, Seymour Island (B). (A) Scanned image showing sedimentary matrix
 1077 cemented by micritic cement cross-cut by putative fluid conduits infilled with multiple generations of
 1078 banded and botryoidal fibrous calcite cement. (B) Scanned image of longitudinal cut through
 1079 carbonate concretion showing micrite cemented sediment cross-cut by putative fluid conduit infilled
 1080 with multiple generations of yellow coloured and translucent banded and botryoidal fibrous calcite
 1081 cement. White box shows area of detail in Fig. 7D. (C,D) QEMSCAN[®] false colour mineralogical
 1082 map based on the fieldscan analysis of thin section; mineralogical key to the colour codes used is
 1083 indicated. (C) Map of the area of the thin section based on a 10 µm beam stepping interval. (D) More
 1084 detailed 5 µm beam stepping interval fieldscan image of area indicated in (C) by white box. Scale
 1085 bars: A-C = 10 mm.

1086

1087 **Fig. 7.** Photomicrographs of petrographic thin sections from concretionary carbonate from sample
 1088 DJ.633.3, Karlsen Cliffs Member, Snow Hill Island (A-C) and carbonate concretion D5.345.2 b1 from
 1089 the López de Bertodano Formation, Seymour Island (D). White arrows in all cases point towards the
 1090 centres of fluid conduits. (A) Centre of fluid conduit infilling showing multiple generations of banded
 1091 and botryoidal fibrous calcite cement (bbc) postdated by equant ferroan calcite (ec); plane polarised
 1092 light image. (B) Centre of fluid conduit infilling showing banded and botryoidal fibrous calcite
 1093 cement (bbc) postdated by probable ankerite cement (an) and then microcrystalline calcite cement
 1094 (m2); plane polarised light image. (C) Fluid conduit showing wall of cemented sedimentary matrix
 1095 (m1) cross-cut by banded and botryoidal fibrous calcite cement (bbc) with complex zonation revealed

1096 by luminescence, and later uniform orange luminescent equant ferroan calcite (ec); CL. (D) Edge of
 1097 fluid conduit infilling showing sequential generations of yellow coloured banded and botryoidal
 1098 fibrous calcite cement (ybbc) and translucent banded and botryoidal fibrous calcite cement (tbbc);
 1099 plane polarised light image. The ybbc phase adjacent to the conduit wall (formed of cemented
 1100 sedimentary matrix - m1) has recrystallized (rbbc), destroying the original fibrous crystal
 1101 aggregations. Scale bars: A,B,D = 500 μm ; C = 200 μm .

1102

1103 **Fig. 8.** Stable carbon and oxygen isotope cross plot from carbonate cemented sediments from Karlsen
 1104 Cliffs Member, Snow Hill Island (SHI) and carbonate concretions from the López de Bertodano
 1105 Formation, Seymour Island (SI).

1106

1107 **Fig. 9.** Gas chromatograms (total ion currents) of hydrocarbon fraction (A) and carboxylic acid
 1108 fraction (B) from Thyasira Hill sample Sn1-1, Karlsen Cliffs Member, Snow Hill Island. Compound-
 1109 specific $\delta^{13}\text{C}$ values are indicated in parentheses. (A) Circles: n-alkanes; black triangles: head-to-tail
 1110 linked isoprenoids; white triangles: tail-to-tail linked isoprenoids; grey triangle: head-to-head-linked
 1111 isoprenoid; PMI: pentamethylcosane; ; istd: internal standard. (B) Circles: n-fatty acids; white
 1112 triangles: iso-fatty acids; black triangle: anteiso-fatty acid; white crosses: α,ω -diacids. C:
 1113 contaminations; istd: internal standard; i: iso; ai: anteiso.

1114 **Tables**

1115 Table 1. Samples examined petrographically and geochemically.

Sample codes	Sample details	Location and reference	Stratigraphical unit	Analytical methods
DJ.616.22 DJ.616.34	' <i>Thyasira</i> ' townsendi specimens	BAS section DJ.616, <i>Thyasira</i> Hill, Snow Hill Island; Lomas (1995)	Karlsen Cliffs Member, Snow Hill Island Formation	Petrography; C and O stable isotopes
Sn1-1, SHI-4, SHI-5, SHI-6, SHI-7	Concretionary sediment with ' <i>Thyasira</i> ' townsendi specimens	<i>Thyasira</i> Hill, Snow Hill Island; this paper	Karlsen Cliffs Member, Snow Hill Island Formation	C and O stable isotopes; organic biomarkers
DJ.731.14	Concretionary sediment	BAS locality DJ.731, Snow Hill Island; Pirrie et al. (1997)	Karlsen Cliffs Member, Snow Hill Island Formation	Petrography; C and O stable isotopes
DJ.633.3	Concretionary sediment	BAS locality DJ. 633.3, Snow Hill Island; Dingle (1995)	Karlsen Cliffs Member, Snow Hill Island Formation	Petrography; C and O stable isotopes
D5.345.2	Carbonate concretions	BAS locality DS. 345.2, Seymour Island; Bowman et al. (2012)	López de Bertodano Formation	Petrography; C and O stable isotopes; XRD analysis

PRI 61054	Cements inside articulated 'Thyasira' townsendi specimen	Zinsmeister collection, locality PU 1478, field no. 89-46	López de Bertodano Formation	Petrography; C and O stable isotopes
PRI 61078	Cements inside articulated 'Lucina' scotti specimen	Zinsmeister collection, locality PU 1478, field no. 89-46	López de Bertodano Formation	C and O stable isotopes
PRI 60596	Cements inside articulated 'Thyasira' townsendi specimen	Zinsmeister collection, locality PU1517, field no. 94-50	López de Bertodano Formation	C and O stable isotopes
PRI 58575	Cements inside articulated 'Thyasira' townsendi specimen	Zinsmeister collection, locality PU K-104	López de Bertodano Formation, Unit KLB 7	C and O stable isotopes

1116

1117 Table 2. Stable isotope data for samples. Carbonate cement phases as used in text.

Sample code	Description	$\delta^{13}\text{C}$	$\delta^{18}\text{O}$
SHI-4B	Cemented sediment matrix (m1)	-18.4	-2.4
SHI-5B	Cemented sediment matrix (m1)	-16.2	-6.6
SHI-6B	Cemented sediment matrix (m1)	-16.2	-3.5

SHI-7A	Cemented sediment matrix (m1)	-14.8	-2.8
sn1-1b	Cemented sediment matrix (m1)	-15.0	-6.0
sn1-1b	Cemented sediment matrix (m1)	-15.6	-5.9
sn1-1a	Cemented sediment matrix (m1)	-15.6	-5.7
sn1-1a	Cemented sediment matrix (m1)	-15.5	-5.6
SHI-4A	'Thyasira' shell	-4.1	-5.5
SHI-5A	Later equant calcite cement (ec)	-12.2	-7.7
SHI-6A	Later equant calcite cement (ec)	-15.9	-5.6
SHI-6C	Later equant calcite cement (ec)	-2.9	-7.6
DJ.731.14	Fibrous calcite cement (bbc)	-15.7	-2.4
DJ.731.14	Fibrous calcite cement (bbc)	-17.2	-2.4
DJ.731.14	Later equant calcite cement (ec)	-10.7	-8.3
DJ.731.14	Fibrous calcite cement (bbc)	-15.7	-2.4
DJ.616.22	Fibrous calcite cement (bbc)	-20.4	-1.6
DJ.616.22	Fibrous calcite cement (bbc)	-11.7	-4.8
DJ.616.22	Later equant calcite cement (ec)	-6.8	-3.0
DJ.633.3	Fibrous calcite cement (bbc)	-14.4	-2.5
DJ.633.3	Fibrous calcite cement (bbc)	-16.4	-2.2
DJ.731.14	Fibrous calcite cement (bbc)	-11.9	-7.0
DJ.731.14	Later equant calcite cement (ec)	-10.8	-8.3
DJ.731.14	Later micro-sparry calcite cement (m2)	-13.5	-5.5

D5.345.2 a	Cemented sediment matrix (m1)	-46.7	0.3
D5.345.2 b1	Fibrous calcite cement (bbc)	-49.3	0.4
D5.345.2 b2	Cemented sediment matrix (m1)	-47.6	0.3
D5.345.2 b3	Fibrous calcite cement (bbc)	-36.1	-2.3
D5.345.2 b4	Fibrous calcite cement (bbc)	-47.0	-1.0
D5.345.2 c	Fibrous calcite cement (bbc)	-51.7	1.2
D5.345.2 d	Cemented sediment matrix (m1)	-47.0	0.2
D5.345.2 e1	Cemented sediment matrix (m1)	-42.4	0.1
D5.345.2 e2	Cemented sediment matrix (m1)	-42.3	0.5
D5.345.2 f	Cemented sediment matrix (m1)	-48.2	0.2
PRI 61054	Infilling fibrous calcite cement (bbc)	-58.0	2.2
PRI 58575	Infilling fibrous calcite cement (bbc)	-27.6	1.9
PRI 60596	Infilling fibrous calcite cement (bbc)	-24.6	0.9
PRI 61078	Infilling fibrous calcite cement (bbc)	-52.5	2.1

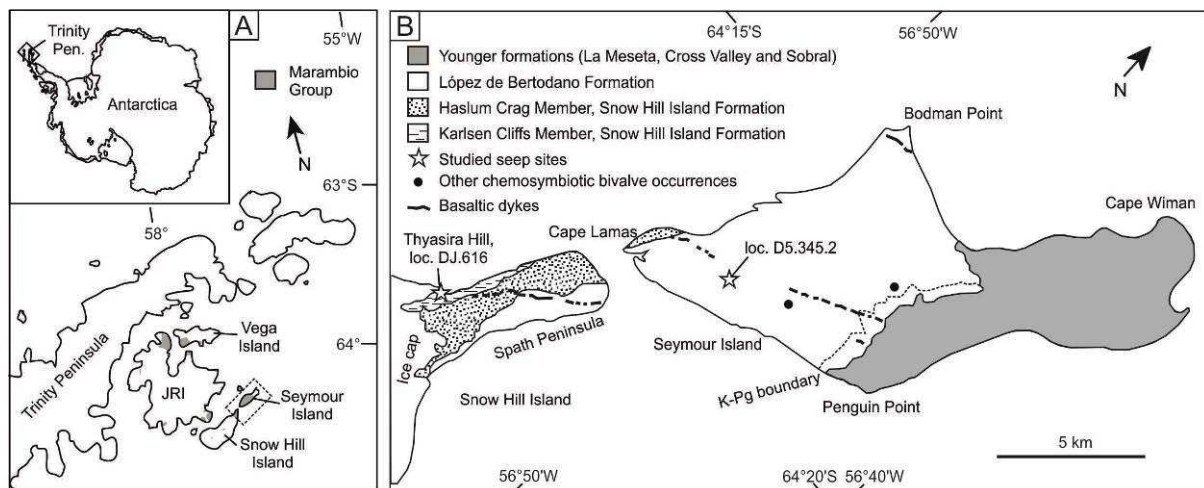


Figure 1

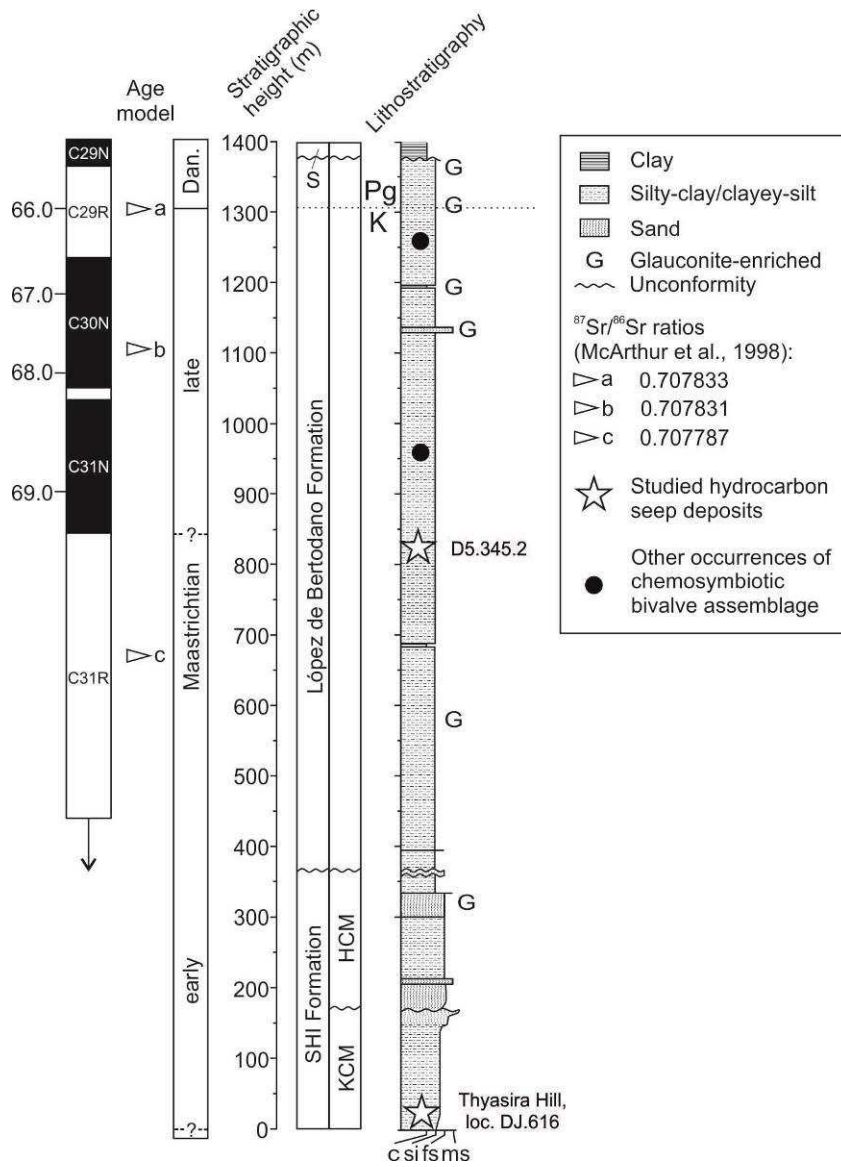


Figure 2

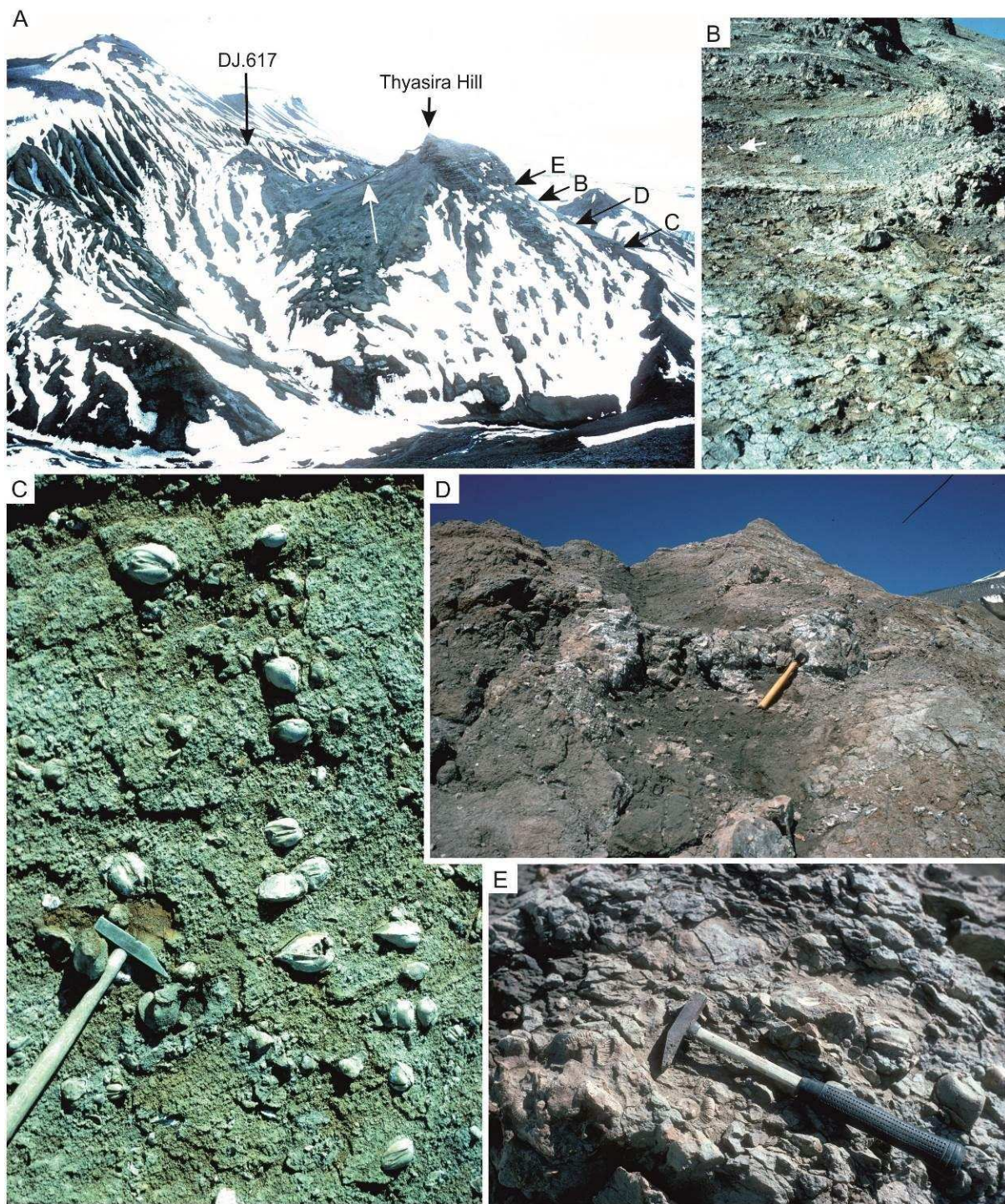


Figure 3

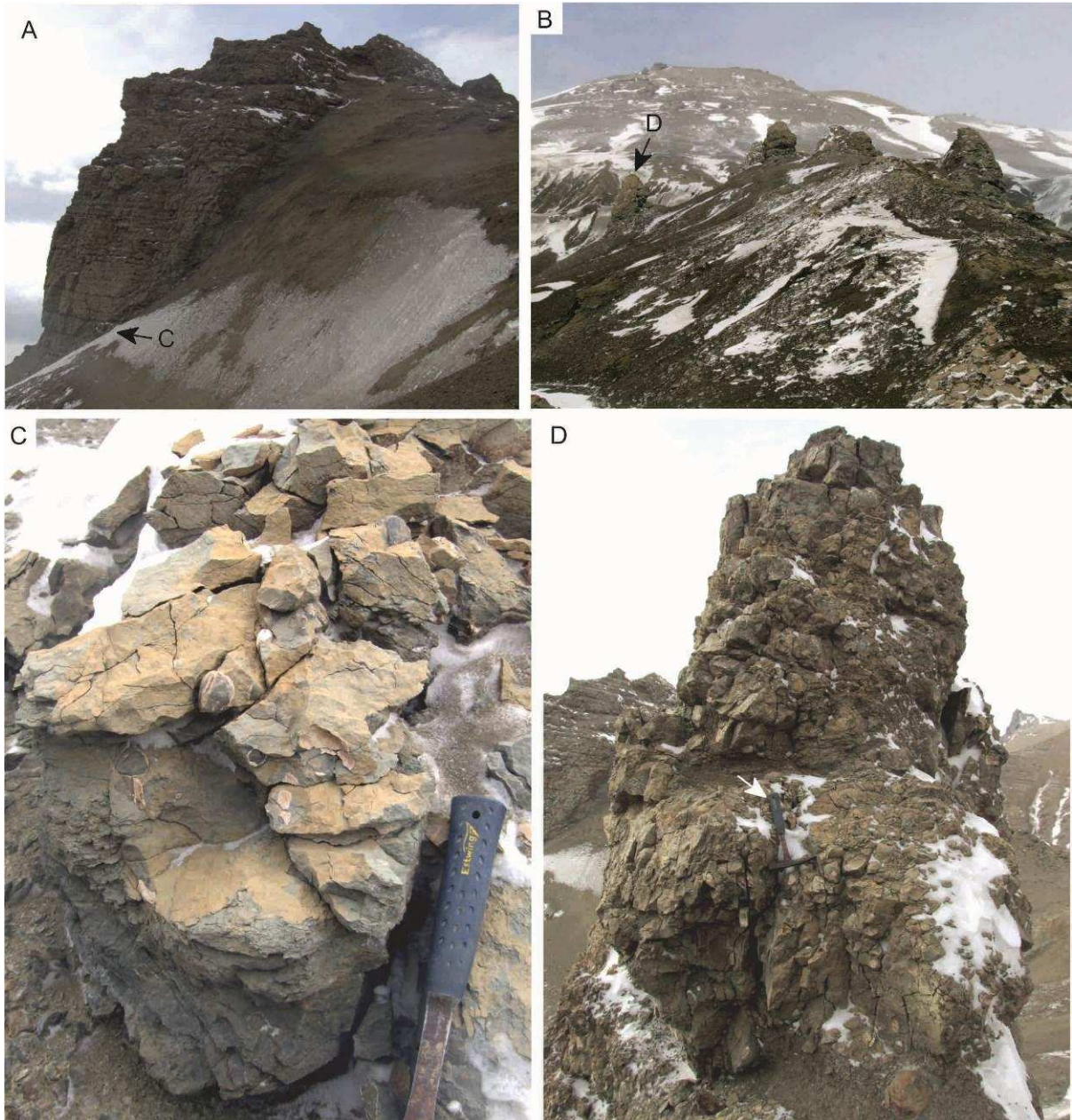


Figure 4

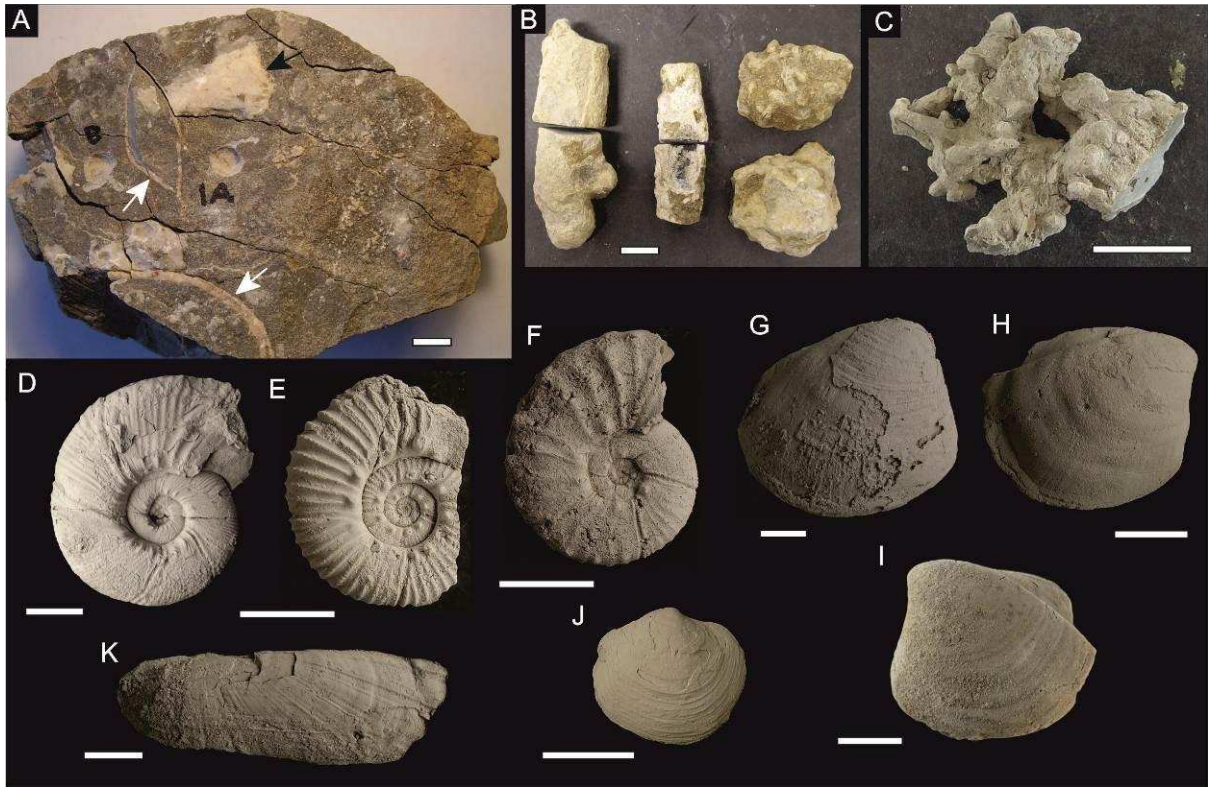


Figure 5

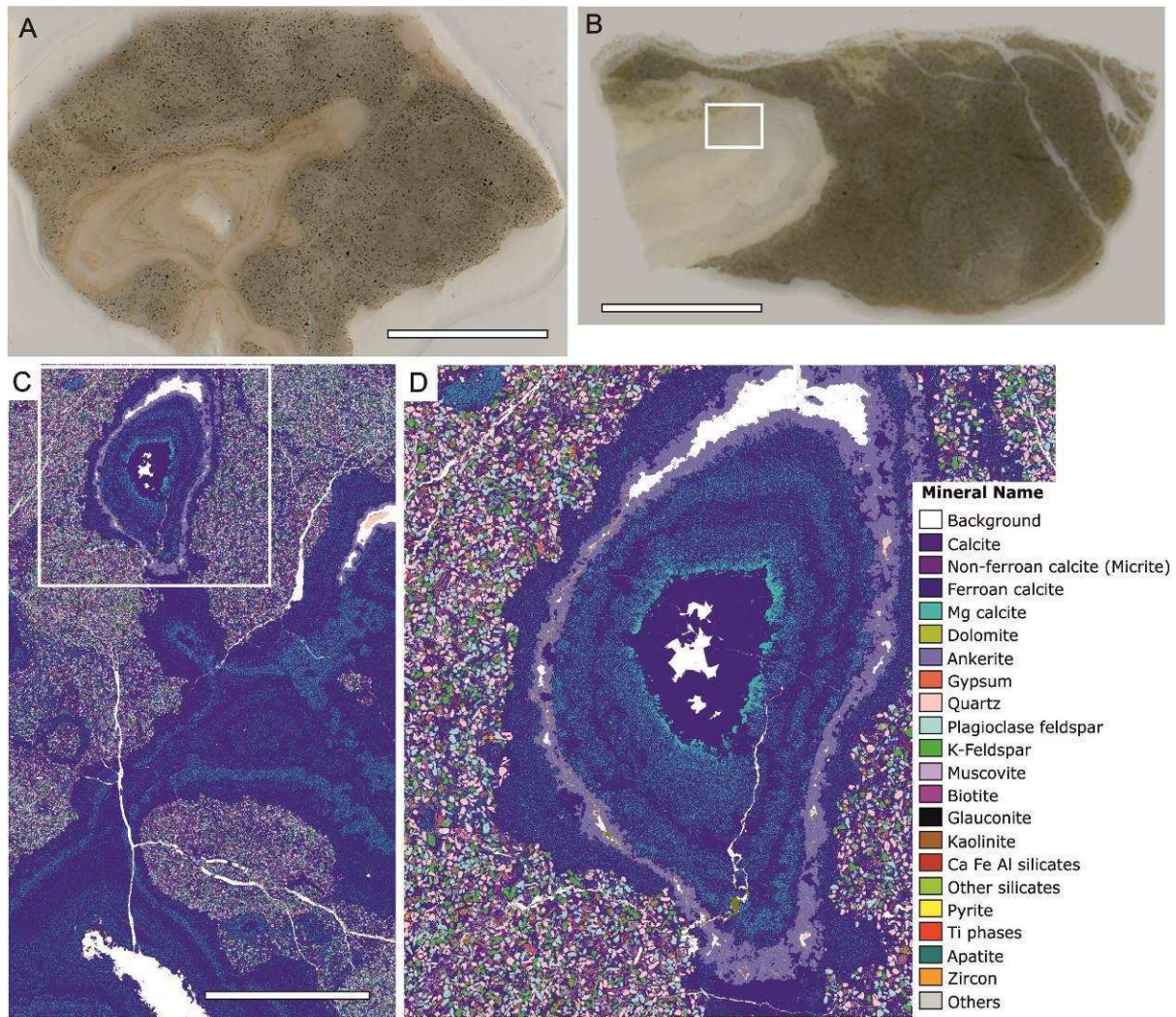


Figure 6

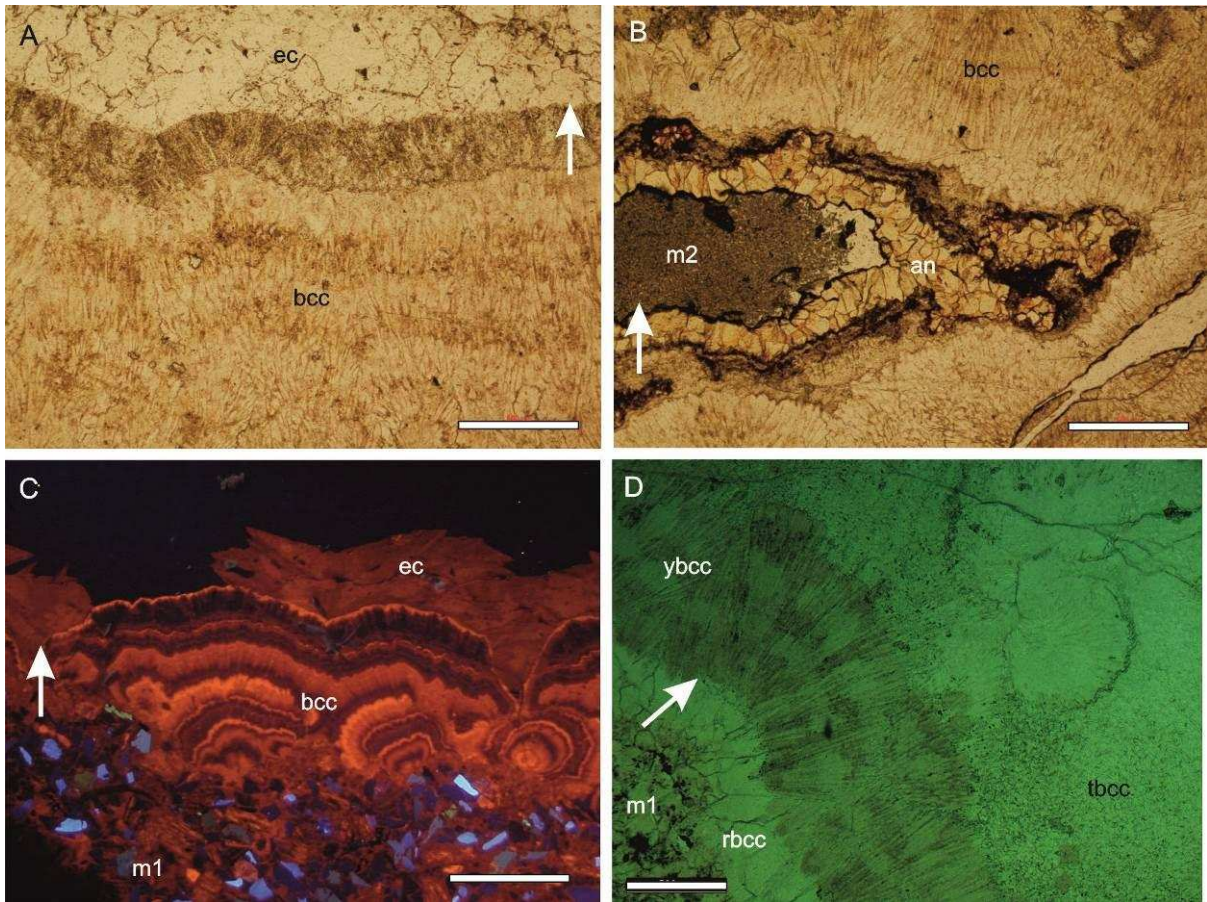


Figure 7

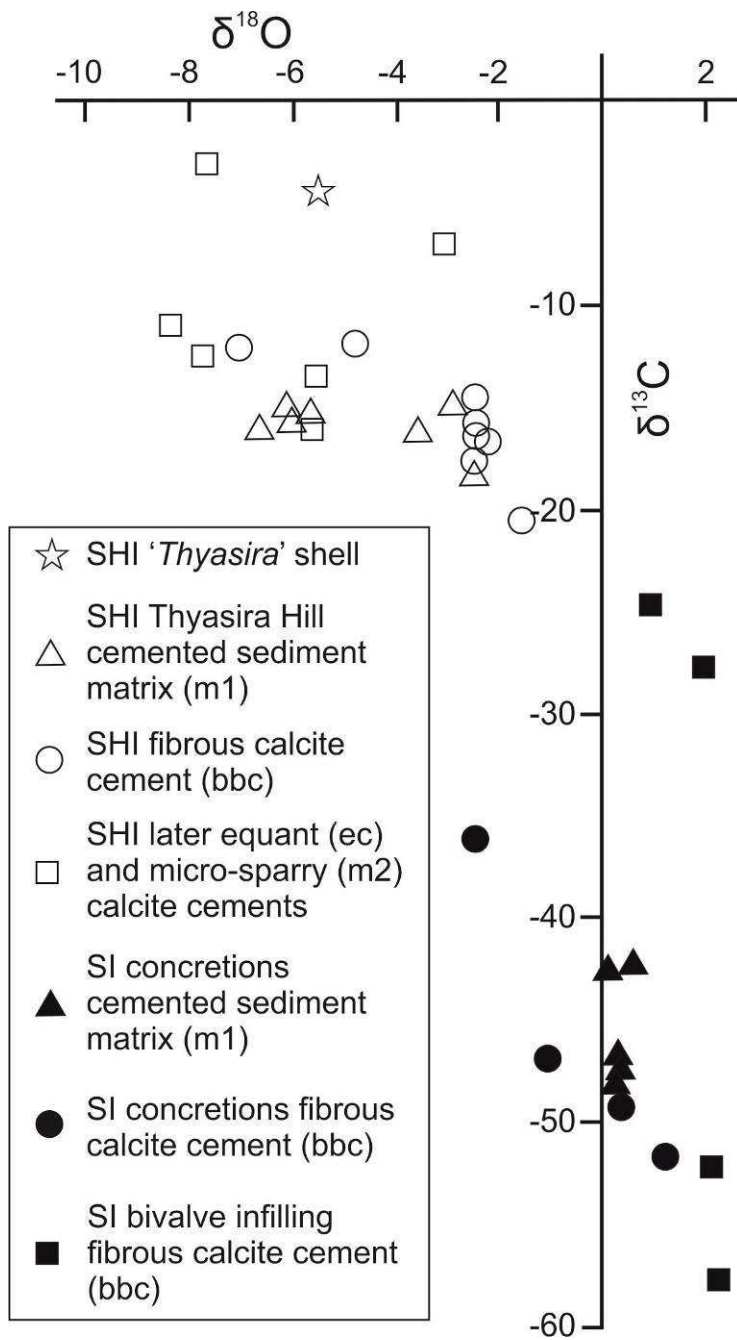


Figure 8

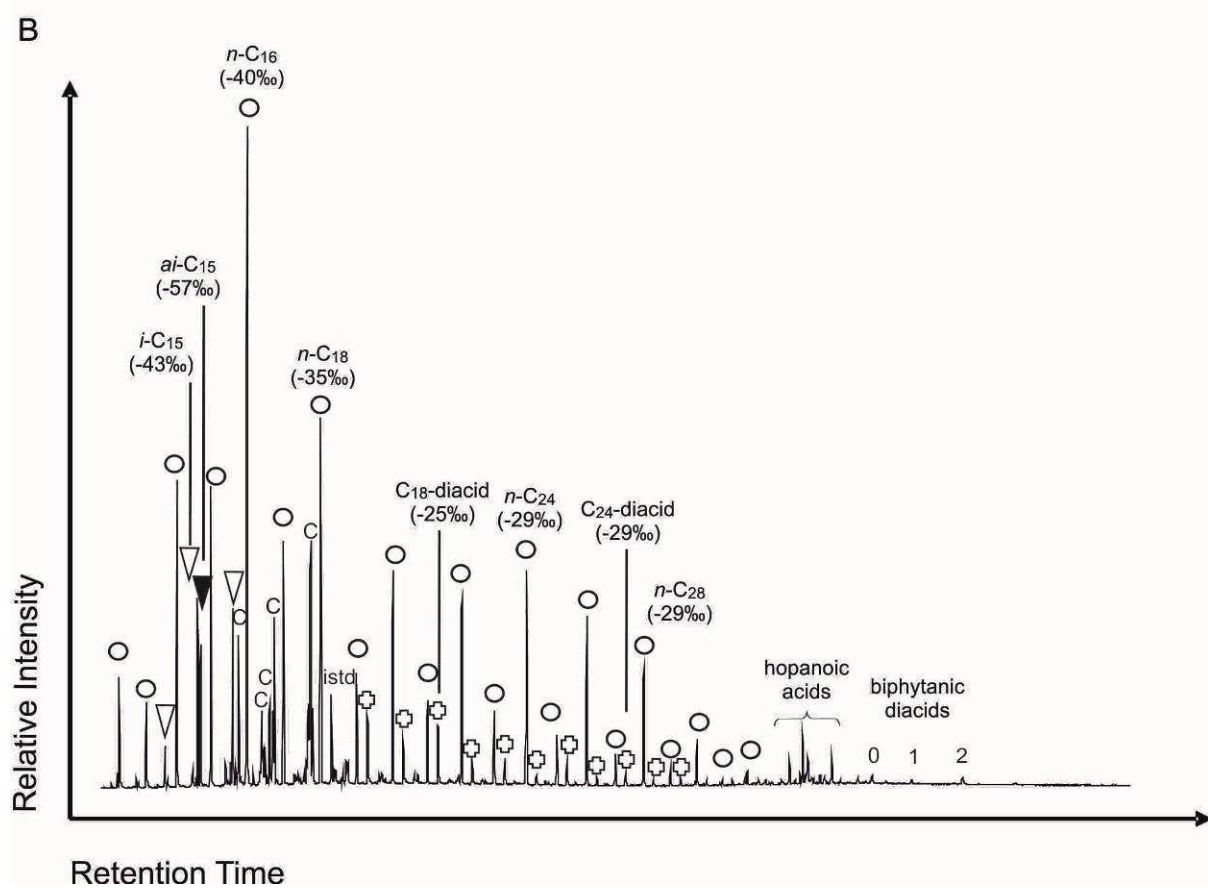
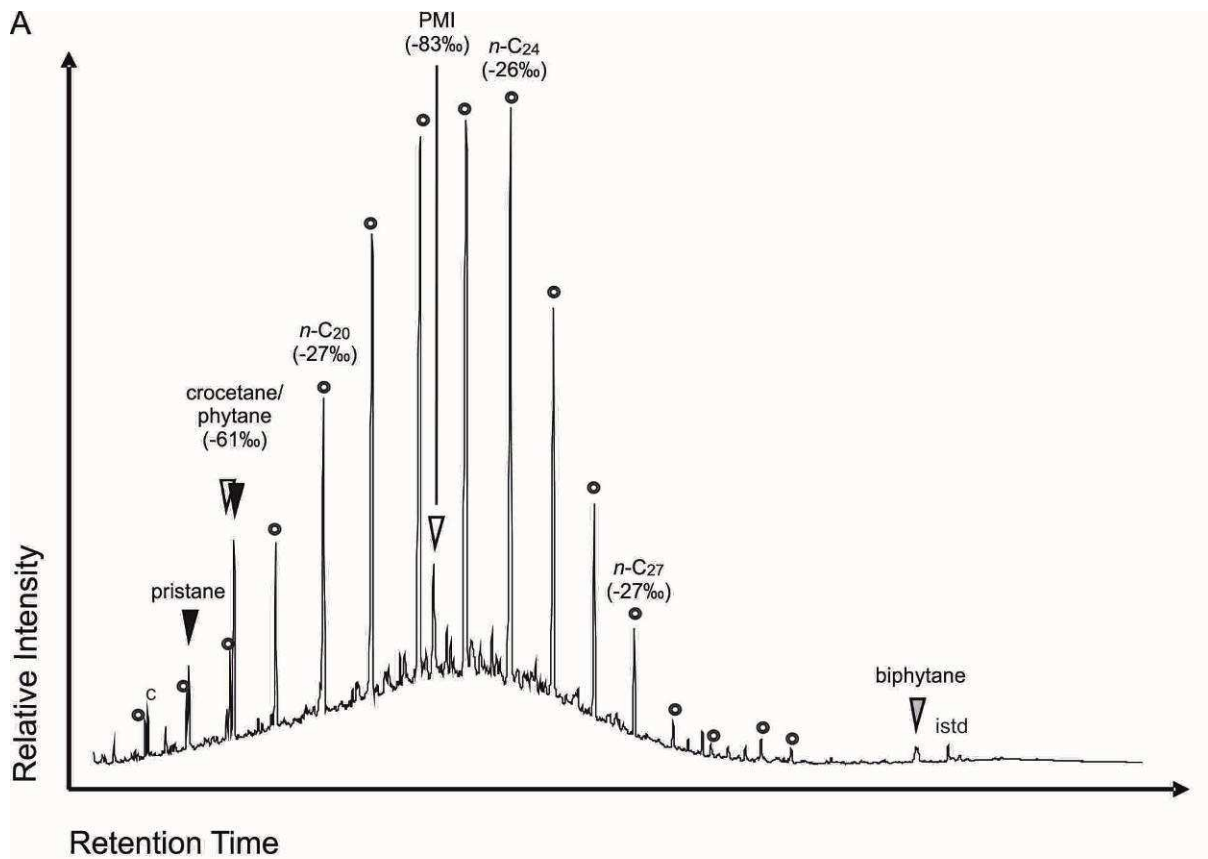


Figure 9